

2005

# Development and analysis of a self-tuned neuro-fuzzy controller for induction motor drives

Wen, Hao

---

<http://knowledgecommons.lakeheadu.ca/handle/2453/3291>

*Downloaded from Lakehead University, Knowledge Commons*

# DEVELOPMENT AND ANALYSIS OF A SELF-TUNED NEURO-FUZZY CONTROLLER FOR INDUCTION MOTOR DRIVES

by  
Hao Wen

A thesis submitted in partial fulfillment  
of the requirements for the degree of  
Master of Science

Lakehead University  
Thunder Bay, Ontario, Canada  
August 2005

© Copyright by Hao Wen, 2005



Library and  
Archives Canada

Bibliothèque et  
Archives Canada

Published Heritage  
Branch

Direction du  
Patrimoine de l'édition

395 Wellington Street  
Ottawa ON K1A 0N4  
Canada

395, rue Wellington  
Ottawa ON K1A 0N4  
Canada

*Your file* *Votre référence*  
*ISBN: 978-0-494-15647-6*  
*Our file* *Notre référence*  
*ISBN: 978-0-494-15647-6*

**NOTICE:**

The author has granted a non-exclusive license allowing Library and Archives Canada to reproduce, publish, archive, preserve, conserve, communicate to the public by telecommunication or on the Internet, loan, distribute and sell theses worldwide, for commercial or non-commercial purposes, in microform, paper, electronic and/or any other formats.

The author retains copyright ownership and moral rights in this thesis. Neither the thesis nor substantial extracts from it may be printed or otherwise reproduced without the author's permission.

**AVIS:**

L'auteur a accordé une licence non exclusive permettant à la Bibliothèque et Archives Canada de reproduire, publier, archiver, sauvegarder, conserver, transmettre au public par télécommunication ou par l'Internet, prêter, distribuer et vendre des thèses partout dans le monde, à des fins commerciales ou autres, sur support microforme, papier, électronique et/ou autres formats.

L'auteur conserve la propriété du droit d'auteur et des droits moraux qui protègent cette thèse. Ni la thèse ni des extraits substantiels de celle-ci ne doivent être imprimés ou autrement reproduits sans son autorisation.

---

In compliance with the Canadian Privacy Act some supporting forms may have been removed from this thesis.

Conformément à la loi canadienne sur la protection de la vie privée, quelques formulaires secondaires ont été enlevés de cette thèse.

While these forms may be included in the document page count, their removal does not represent any loss of content from the thesis.

Bien que ces formulaires aient inclus dans la pagination, il n'y aura aucun contenu manquant.

  
**Canada**

# Abstract

Induction motors (IM) have been widely utilized in industry for variable speed drives due to some of their advantages, such as rugged construction, low cost and reliable service with easy maintenance, as compared to conventional dc motors. For variable speed drive applications, the controller plays an important role so that the motor can follow the reference trajectories without any significant deviation. Furthermore, a controller which can provide fast speed response and handle uncertainties and disturbances, is absolutely necessary for high performance drive systems. Traditionally, fixed gain proportional-integral (PI) and some adaptive controllers have been utilized in industry for a long time. However, there are some disadvantages of these controllers to handle uncertainties which are inherent to a nonlinear IM. As a result, recently researchers paid their attention to apply intelligent algorithms to control the IM for high performance variable speed drive applications. Intelligent algorithms such as fuzzy logic (FL), neural network (NN), neuro-fuzzy (NF), etc, have inherent advantages as compared to the conventional controllers.

In this thesis, a novel neuro-fuzzy controller (NFC) has been developed for speed control of IM. For the complete drive, the indirect field orientation control is utilized in order to decouple the torque and flux controls. Thus, the induction motor can be controlled like a dc motor and hence the high performance can be achieved without lacking the advantage of ac over dc motors. The proposed neuro-fuzzy controller incorporates Sugeno model based fuzzy logic laws with a five-layer artificial neural

network (ANN) scheme. The controller is designed for low computational burden, which will be suitable for real-time implementation. Furthermore, for the proposed NFC an improved self-tuning method is developed based on the IM theory and its high performance requirements. The main task of the tuning method is to adjust the parameters of the fuzzy logic controller (FLC) in order to minimize the square of the error between actual and reference output. In this thesis, a model reference adaptive flux (MRAF) observer is also developed to estimate the d-axis rotor flux linkage in both constant flux and flux weakening regions based on motor voltage, current and reference trajectories for flux linkage. Thus, it provides safe operation to control the motor at high speeds, especially, above the rated speed. The d-axis reference flux linkage of the indirect field oriented control is provided by flux weakening method. Furthermore, a proportional-integral (PI) based flux controller is used to provide the compensation for the reference flux model by comparing the flux reference and the observed flux from Gopinath model flux observer. A complete simulation model for indirect field oriented control of IM incorporating the proposed MRAF observer based NFC is developed in Matlab/Simulink. In order to prove the superiority of the proposed controller, the performance of the proposed controller is compared with a conventional PI as well as fuzzy logic controller (FLC) based IM drives. The performance of the proposed IM drive is investigated extensively at different operating conditions in simulation. The performance of the proposed MRAF observer based NFC controller is found robust and a potential candidate for high performance industrial drive applications.

# Acknowledgements

I would like to express my most sincere gratitude and appreciation to my supervisor Dr. M. Nasir Uddin for his guidance, advice and encouragement throughout of this program.

I would like to extend my appreciation to the Faculty of Engineering at Lakehead University, all Faculty members, staff members and fellow graduate students.

I am deeply grateful to Ms. Ying Sun for her sacrifice and love.

Finally, I express my sincere appreciation to my parents, Ms. Fengying Guo and Mr. Guoxin Wen, as well as other family members and friends without whose support and encouragement it would not have been possible to complete this work.

# Contents

<b>Abstract</b>	<b>ii</b>
<b>Acknowledgement</b>	<b>iv</b>
<b>Contents</b>	<b>v</b>
<b>List of Figures</b>	<b>vii</b>
<b>List of Symbols</b>	<b>xi</b>
<b>List of Acronyms</b>	<b>xiii</b>
<b>1 Introduction</b>	<b>1</b>
1.1 Induction Motors.....	2
1.2 Field Orientation Control.....	4
1.3 Literature Search.....	6
1.3.1 PI, PID and Adaptive Controllers.....	6
1.3.2 Intelligent Controllers.....	8
1.4 Motivation.....	12
1.5 Thesis Organization.....	13
<b>2 Closed Loop Field Orientation Control of Induction Motors</b>	<b>15</b>
2.1 Coordinate Transformations.....	16
2.2 Mathematical Model of IM.....	19
2.3 Field Orientation Control.....	22
2.4 Voltage Source Inverter.....	24
2.5 Speed Controller.....	28
2.6 Hysteretic Current Control.....	29

2.7	Summary.....	31
<b>3</b>	<b>Development of Neuro-Fuzzy Controller</b>	<b>32</b>
3.1	Fuzzy Logic Control.....	33
3.1.1	Fuzzification.....	34
3.1.2	Fuzzy Inference Engine.....	35
3.1.3	Defuzzification.....	35
3.2	Neural Network.....	36
3.3	Design of Neuro-fuzzy Controller.....	39
3.3.1	Detailed Structure of NFC.....	40
3.3.2	Tuning Method .....	43
<b>4</b>	<b>Simulation of NFC based FOC of IM drive</b>	<b>47</b>
4.1	Drive System.....	47
4.2	Simulation Results and Discussion.....	48
4.3	Summary.....	68
<b>5</b>	<b>Design of Model Reference Adaptive Rotor Flux Observer</b>	<b>69</b>
5.1	Closed Loop Flux Observer Model.....	70
5.2	MARF Rotor Flux Regulation.....	71
5.3	Simulation of the MRAF observer based NFC for IM drive.....	73
5.4	Experimental Setup.....	74
<b>6</b>	<b>Conclusion</b>	<b>79</b>
6.1	Achievements of the Thesis.....	80
6.2	Future Scope of the Work.....	81
	<b>Appendix A</b>	<b>82</b>
	<b>Appendix B</b>	<b>84</b>
	<b>Bibliography</b>	<b>92</b>



# List of Figures

1.1	(a) Wound-rotor induction motor (b) Squirrel-cage induction motor.....	3
1.2	Block diagram of a FOC based IM drive.....	5
2.1	Relative positions of a-b-c, stator and excitation reference frame.....	17
2.2	Dynamic equivalent circuit of induction motor.....	20
2.3	Closed loop indirect FOC scheme.....	24
2.4	Circuit diagram of a three-phase VSI.....	25
2.5	Space vectors of output voltages of a VSI.....	27
2.6	Block diagram of a current-controlled VSI for IM drive.....	30
2.7	Input-output characteristic of a hysteretic current controller.....	30
3.1	Block diagram of fuzzy logic control.....	34
3.2	The example of membership function and fuzzification.....	34
3.3	The example of expressing a set of rules and defuzzification.....	36
3.4	The example of a typical structure of neural network.....	37
3.5	Structure of the NF controller.....	39
3.6	Membership functions of inputs: (a) 3 membership functions scheme, and (b) 2 membership functions scheme.....	41
3.7	Design reference of $d\omega/dt$ .....	45

3.8	Comparison of current $i_a$ , torque and steady-state speed response, respectively, under conditions of different $\eta$ : (a) current $i_a$ , (b) torque, and (c) speed.....	46
4.1	Proposed NFC based IM drive.....	48
4.2	Simulated starting responses of the drive with NFC: (a) speed, (b) current $i_a$ , (c) torque, and (d) stator frame $i_d$ versus $i_q$ response.....	53
4.3	Simulated starting responses of the drive with NFC at full torque (150 N.m) and rated speed (180 rad./sec.) conditions: (a) speed, and (b) actual a-phase current.....	54
4.4	Simulated starting responses of the drive with NFC at full load (150 N.m) and $\omega^*=100$ rad./sec.: (a) speed, and (b) current $i_a$ .....	55
4.5	Simulated starting responses of the drive with NFC at full load (150 N.m) and low command speed (30 rad./sec.) conditions: (a) speed, and (b) current $i_a$ ...	56
4.6	Simulated responses of the drive with NFC for a step increase in load ( 0N.m $\rightarrow$ 150N.m): (a) speed, and (b) torque.....	57
4.7	Simulated speed responses of the drive with PI for a step increase in load ( 0N.m $\rightarrow$ 150N.m).....	58
4.8	Simulated speed responses of the drive with FLC for a step increase in load ( 0N.m $\rightarrow$ 150N.m).....	58
4.9	Simulated speed response of the drive at full load with NFC for a sinusoidal speed reference.....	59
4.10	Simulated speed response of the drive at full load with PI controller for a sinusoidal speed reference.....	59

4.11	Simulated speed response of the drive at full load with FLC for a sinusoidal speed reference.....	60
4.12	Speed response of the proposed drive at full load for speed reversal.....	60
4.13	Simulated responses of the NFC based drive at full load for speed reversal: (a) torque, and (b) $\Delta\omega$ .....	61
4.14	Simulated responses of the FLC based drive at full load for speed reversal: (a) speed, (b) torque and (c) $\Delta\omega$ .....	62
4.15	Simulated speed response of the proposed NFC based drive at rated load for doubled magnetizing inductance: (a) speed, and (b) current $i_a$ .....	63
4.16	Simulated speed response of the proposed NFC based drive at rated load for doubled $J_m$ : (a) speed, and (b) current $i_a$ .....	64
4.17	Simulated speed response of the proposed NFC based drive at rated load for doubled rotor resistance: (a) speed, and (b) current $i_a$ .....	65
4.18	Simulated starting responses of the proposed NFC based 3HP IM drive without load: (a) current $I_a$ , (b) torque, and (c) speed.....	66
4.19	Simulated starting responses of the drive with 2 membership functions NFC without load: (a) current $I_a$ , (b) torque, and (c) speed.....	67
5.1	Closed loop Gopinath flux observer.....	71
5.2	Proposed MRAF observer.....	73
5.3	Simulated starting responses of the proposed MRAF based NFC for IM drive with $T_L=150$ N.m; (a) speed, (b) flux, (c) current $i_a$ , and (d) torque.....	75

5.4	Simulated responses of the drive of MRAF based NFC for a high speed command of 300rad/s without a nonlinear load; (a) speed, (b) torque, and (c) flux.....	76
5.5	Simulated responses of the drive of MRAF based NFC for a high speed command of 300rad/s without load=100 N.m; (a) speed, (b) torque, and (c) flux. ....	77
5.6	Block diagram of the hardware schematic of the VSI-fed IM drive.....	78
B.1	Proposed NFC Subsystem.....	85
B.2	NFC Training Subsystem.....	86
B.3	Flux Observer Subsystem.....	87
B.4	MRAF Subsystem.....	88
B.5	Coordinate Transformation Subsystem.....	89
B.6	Hysteretic Current Controller Subsystem.....	90
B.7	Real-Time Simulink Model for the NFC based IM drive.....	91

# List of Symbols

$i_a, i_b$ and $i_c$	Actual a, b and c, phase currents, respectively
$i_a^*, i_b^*$ and $i_c^*$	Command a, b and c, phase currents, respectively
$v_a, v_b$ and $v_c$	a, b and c, phase voltages, respectively
$i_s^s$	Vector of stator current in the stator reference frame
$i_{ds}^s$ and $i_{qs}^s$	d-axis and q-axis stator currents, respectively.
$i_{dr}^s$ and $i_{qr}^s$	d-axis and q-axis rotor currents, respectively.
$v_{ds}^s$ and $v_{qs}^s$	d-axis and q-axis stator voltages, respectively.
$v_{dr}^s$ and $v_{qr}^s$	d-axis and q-axis rotor voltages, respectively.
$v_s^s$	Vector of stator voltage in the stator reference frame
$i_r^s$	Vector of rotor current in the stator reference frame
$R_s$	Stator resistance
$R_r$	Rotor resistance.
$\lambda_s^s$	Vector of stator flux
$\lambda_r^s$	Vector of rotor flux
$\omega_r$	Rotor speed

$\omega_{sl}$	Slip speed of a motor
$\omega_r^*$	Command speed
$p$	Differential operator.
$L_s$	Self inductance of stator
$L_r$	Self inductance of rotor
$L_m$	Mutual inductance
$P$	Number of pole-pairs
$\lambda_{dr}^e$ and $\lambda_{qr}^e$	d-q axes rotor flux linkage in the excitation reference frame.
$T_e^*$	Command torque
$\lambda_r^*$	Command rotor flux
$\theta_e$	Synchronous electrical angle
$T_L$	Load torque
$K_p$	Proportional constant
$K_i$	Integral constant

# List of Acronyms

IM	Induction motors
PI	Proportional-integral
FL	Fuzzy logic
NN	Neural network
ANN	Artificial neural network
GA	Genetic algorithm
NF	Neuro-fuzzy
NFC	Neuro-fuzzy controller
FLC	Fuzzy logic controller
MRAF	Model reference adaptive flux
FOC	Field orientation control
e.m.f.	Electromotive force
MRAC	Model reference adaptive controller
PWM	Pulse width modulation
VSI	Voltage source inverter
BJT	Bipolar junction transistor
AI	Artificial intelligence

# Chapter 1

## Introduction

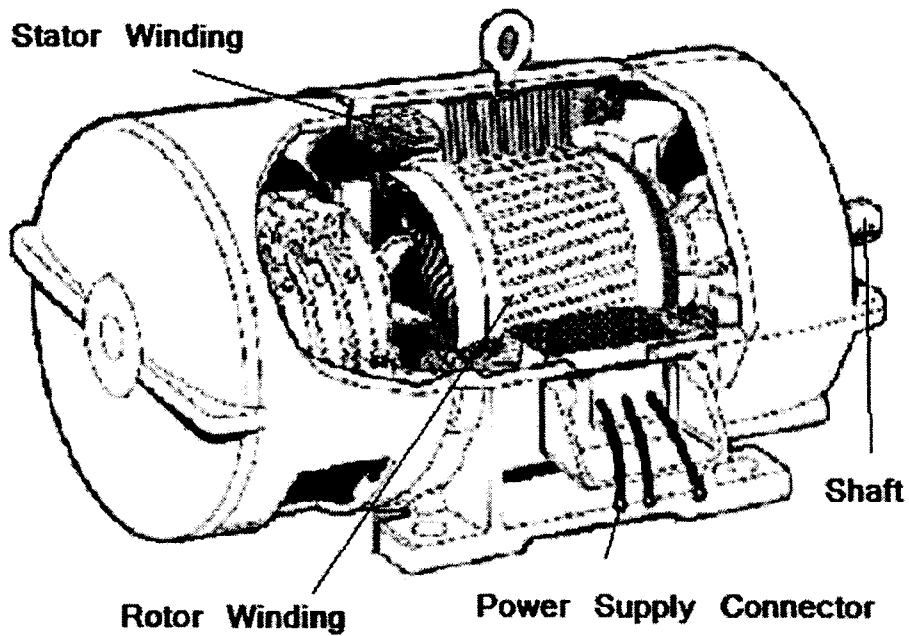
Early days, only dc motors were utilized for high performance variable speed drive applications in industry. However, disadvantages of dc motors are apparent, such as high cost, high maintenance requirement and limited speed range. In order to overcome these disadvantages, researchers looked into ac motors for variable speed drive applications.

The induction motor is widely used in industry due to its ruggedness, reliability and easy maintenance [1-3]. The field orientation control (FOC) technology decouples the flux and torque control in an IM, thus makes high performance IM drive theoretically feasible [4-8]. With the advent of recent power semiconductor technologies and various intelligent control algorithm, effective control methods based on vector control technology can be fully implemented in real time application, thus induction motors can competently be used for high performance variable speed drive applications.

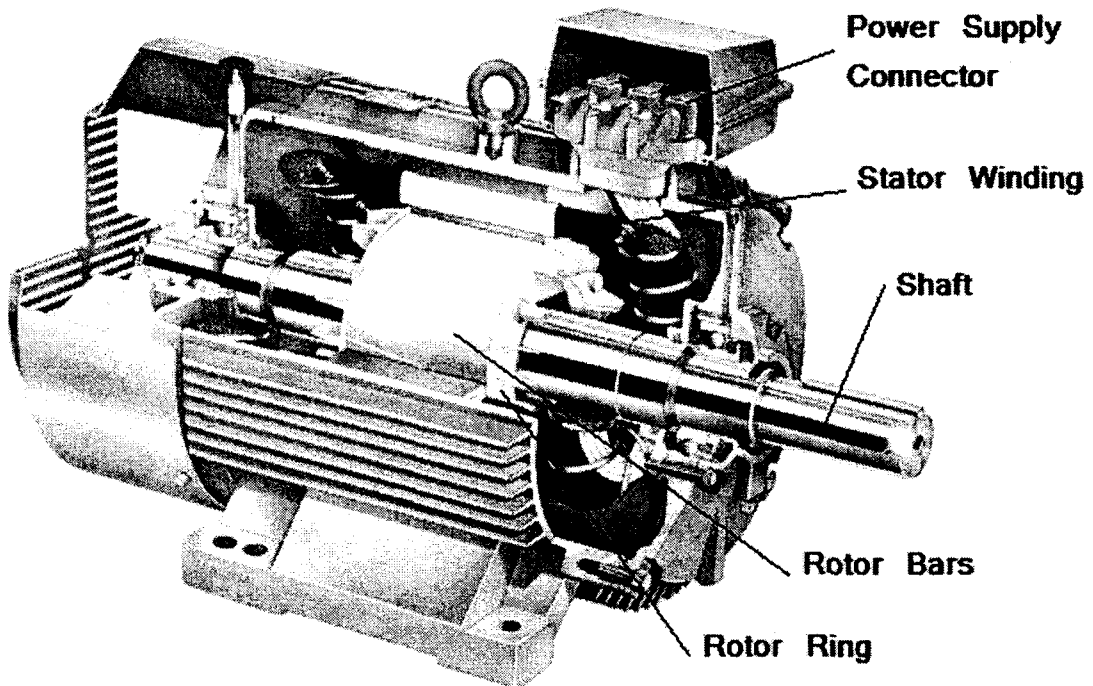


# 1.1 Induction Motors

Electric motors convert electrical energy into mechanical motion and are widely used in both industry and home appliances. Now-a-days, the polyphase asynchronous ac motor, also well-known as the induction motor (IM) is one of the most popular machines employed in industrial drives, owing to its simple and rugged design, low cost and reliable service with easy maintenance. There are two different types of induction motors classified by the rotor type, such as squirrel-cage induction motor and wound-rotor induction motor [1]. The rotor of a squirrel-cage induction motor consists of a bunch of conducting bars shorted at both ends by shorting rings, which are embedded into slots in the rotor. Fig. 1.1 shows the sectional view of squirrel-cage and wound rotor IM. Instead of using conducting bars, a wound-rotor induction motor employs a complete set of polyphase windings as its rotor. An advantage of the wound-rotor IM is indicated that various performance characteristics can be obtained by inserting different values of resistance in the rotor circuit. On the other hand, there are some disadvantages of wound rotor IM due to its rotor slip rings and brushes. However, both squirrel-cage induction motor and wound-rotor induction motor perform the same fundamental functions. Considering the relative advantage of squirrel-cage IM due to its simple construction and easy maintenance, this motor is considered for the present work. In an IM, the rotor flux is produced by the rotor-induced voltage which depends on the slip frequency. Due to the difference in speed between rotor and rotating magnetic field produced by stator currents the control of an IM is relatively complex and it requires sophisticated control strategy.



(a)



(b)

Fig. 1.1: (a) Wound-rotor induction motor (b) Squirrel-cage induction motor

## 1.2 Field Orientation Control

The concept of field orientation control (FOC) was first introduced by Haase and Blaschke in the early seventies [4] for high performance variable speed drive applications. At first, their methods seemed impractical due to an insufficient means of implementation. However, with the advent of recent power semiconductor technologies and microprocessor-based control systems, effective control method based on FOC technology can be fully implemented in real time application, thus induction motors can competently be used for high performance variable speed drive applications.

In a separately-excited dc motor, independent control of the torque and field flux is feasible by means of controlling the current in rotor armature winding and the current in field winding separately. In a similar manner to that in dc machines, in induction motors the armature winding is also on the rotor, while the field is generated by currents in the stator winding. However, the rotor current is not directly derived from an external source but results from the electromotive force (e.m.f.) induced in the winding as a result of the relative motion of the rotor conductors with respect to the stator field. In other words, the stator current is the source of both the rotating magnetic field and rotor current. In the most commonly used squirrel-cage motors, only the stator current can be directly controlled, since the rotor winding is not accessible. Optimal torque production conditions are not inherent due to the absence of a fixed physical disposition between the stator and rotor fields, and hence

the torque is nonlinear. In effect, independent and efficient control of the field and torque is not as simple and straightforward as in dc motors.

A field orientation control (FOC) for IM emulates a separately-excited dc motor so that both the magnetic field and the torque developed in the motor can be controlled independently [5-8]. Thus, FOC-IM can competently be used for high performance variable speed drive applications. The block diagram of a typical FOC based IM drive is shown in Fig 1.2.

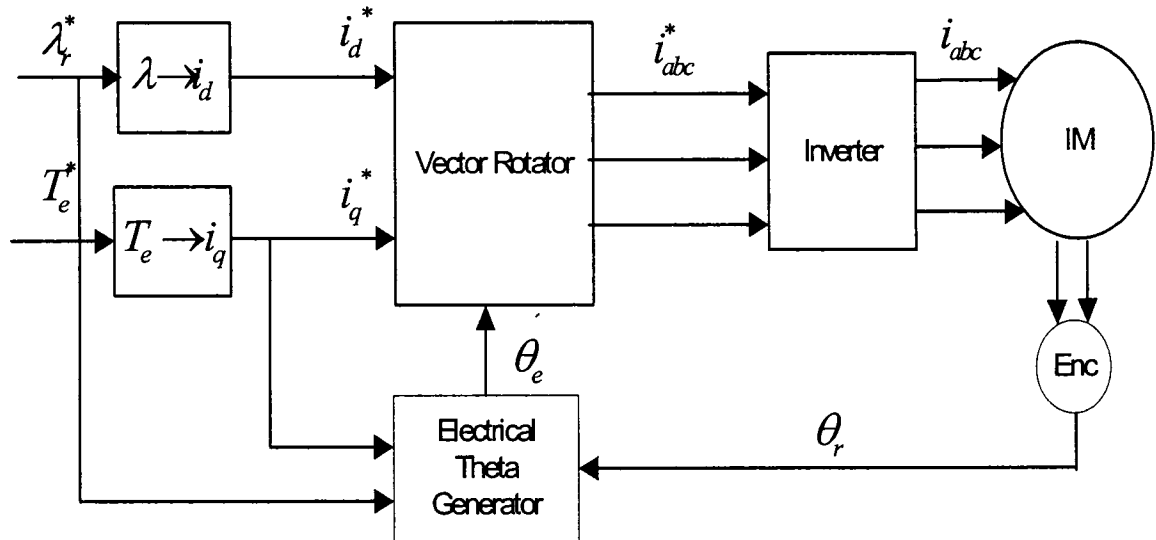


Figure 1.2: Block diagram of a FOC based IM drive

## 1.3 Literature Search

### 1.3.1 PI, PID and Adaptive Controllers

Traditionally industrial controls of IM utilize proportional-integral (PI), proportional-integral-derivative (PID) and their adaptive versions [9-14]. The conventional PI and PID have been used as the speed controller for the IM drive for the last few decades, because of their simplicity and ease to implement in real time [9-10]. However, these controllers are very sensitive to parameter variations due to saturation, temperature variation, sudden change of command speed, load disturbances and other uncertainties [9]. Moreover, it is difficult to tune the controller parameters exactly both for online and off-line implementations. Therefore, these types of controllers are not always suitable for high performance applications. As a result, researchers [11-14] have developed adaptive control schemes for IM drive systems so that the controller can adapt the controller parameters to system parameter variations and load disturbances. The availability of relatively inexpensive and powerful digital signal processors (DSP) has encouraged researchers to apply these adaptive controllers for IM drives.

Recently, adaptive controllers have been used for IM drives to achieve fast transient response, parameter insensitivity, nonlinear load handling capability and high adaptability to other types of uncertainties. Among various adaptive schemes, the model reference adaptive controller (MRAC) scheme is one in which the drive forces the response to follow the output of a reference model regardless of the drive

parameter changes [11]. MRAC may be used with a PI controller to adapt the controller gains as a compensation to the system parameter changes. It is impossible to adapt the controller gains exactly, so the parameters are adapted by trial and error such that the error between the actual and the desired responses remains within the specified limit. The reference model is designed by considering the worst case system parameters so that the drive can physically track the reference model. Leksono,E, and Pratikto [11] have reported a vector control based IM drive using MRAC. In that work, the inner current control loops are realized with proportional and integral controllers while for the outer loop, the adaptive controller derivation is based on a class of MRAC where the reference model is chosen as first order system.

Backstepping control is a relatively new technique for the control of uncertain nonlinear systems. The most appealing point is the use of virtual control variables to make the original high order system simple, thus the final control outputs can be derived step by step through suitable Lyapunov functions ensuring global stability. In [12] the authors have reported an adaptive backstepping control method for a speed sensorless FOC-IM drive. Full state variable information together with exact parameter knowledge is needed for traditional speed control based IM drive. The aim of [12] is to fulfill these needs by use of a nonlinear observer structure based on the backstepping principle. The authors of [13] combined field orientation and adaptive backstepping approach for the control of induction motors. Parameter uncertainties of the rotor resistance and load torque disturbance are compensated using adaptive backstepping control techniques.

In [14] a recursive adaptation algorithm for rotor resistance applied to nonlinear feedback controller is also presented. In this paper some simulation results show that the adaptation algorithm for rotor resistance is robust against the variation of stator resistance and mutual inductance. However, it is well-known that the designs of these adaptive controllers depend on accurate system mathematical model, which is impossible to develop for a nonlinear induction motor.

### 1.3.2 Intelligent Control

Due to the mentioned disadvantages of conventional PI, PID and some adaptive controllers, recently researchers paid their attentions to applying intelligent algorithms for motor drive applications [15-43]. There are some advantages of intelligent controllers as compared to conventional PI, PID and some adaptive controllers, such as the design of intelligent controllers are independent of the detailed system model with accurate parameters, and it can handle nonlinearity of arbitrary complexity. The popular intelligent algorithms utilized for motor drives are fuzzy logic control (FLC) [28-35], artificial neural network (ANN) [17-26], neuro-fuzzy control (NFC) [36-43] and genetic algorithm (GA) [15-16].

Researchers [15] applied GA for motor drive applications. However, the computing burden with GA is really high and hence it cannot be applied on-line. The reported works [16] applied GA only to optimize some of the controller parameters off-line.

Some work has already been reported on the use of artificial neural networks (ANNs) for dc motor drives [17-19] and induction motor drives [20-26]. Weerasooriya and El-Sharkawi [17] have developed an ANN based dc motor drive. They have used the back-propagation training algorithm. In this work, two types of controller topologies are developed. For both topologies two artificial neural networks are used. The authors in [25] presents ANN approach to the FOC of IM drives. It discusses the introduction of artificial neural networks (ANNs) for decoupling control of induction motors using FOC principles. Two ANNs are presented for direct and indirect FOC applications. The first performs an estimation of the stator flux for direct field orientation, and the second is trained to map the nonlinear behavior of a rotor-flux decoupling controller. In [26], the authors proposed a robust speed control method for induction motor drives based on a two-layered neural network plant estimator and a two-layered neural network PI controller. The NN plant estimator is used to provide a real-time adaptive estimation of the unknown motor dynamics. The widely used projection algorithm is used as the learning algorithm for these neural networks to automatically adjust the parameters of the NN PI controller and to minimize the differences between the motor speed and the speed predicted by the NN plant estimator.

In order to obtain a more flexible and effective capability of handling and processing the uncertainties of a complicated nonlinear system like IM drive, Zadeh [27] proposed a linguistic approach, which introduced the fuzzy set and fuzzy logic theory. Thus, a fuzzy logic controller (FLC) is developed. Human thinking is often qualitative rather than quantitative, involving the ideas like high, low, medium etc.



Presently, researchers [28-31] have developed fuzzy logic controllers for motor drives to mimic human thinking as closely as possible. Some work has already been reported on the use of a FLC for induction motor drives [32-35]. In [32] the authors proposed adaptive scheme uses a Takagi-Sugeno fuzzy controller, which allows the inclusion of a priori information in terms of qualitative knowledge about the plant operating points or analytical conventional regulators for those operating points. The proposed approach performance is evaluated on an induction motor control problem. In [33] the authors presents a speed control scheme of an induction motor (IM) using fuzzy-logic control. The fuzzy-logic controller (FLC) is based on the indirect vector control. The fuzzy-logic speed controller is employed in the outer loop. In this work, the performances of the proposed FLC-based IM drive are investigated and compared to those obtained from the conventional proportional-integral (PI) controller-based drive both theoretically and experimentally at different dynamic operating conditions such as sudden change in command speed, step change in load, etc.

However, either fuzzy logic control or artificial neural network has its own drawbacks, which cannot be avoided and neglected. A simple fuzzy controller implemented in the motor drive speed control has a narrow speed operation and needs much manual adjusting by trial and error if high performance is wanted [16]. On the other hand, it is extremely tough to create a serial of training data for ANN that can handle all the operating modes. The neuro-fuzzy hybrid system combines the advantages of fuzzy logic systems, which deal with explicit knowledge that can be explained and understood, and artificial neural networks, which deal with implicit knowledge by means of either off-line parameters training or online parameters

training. Researchers [36-43] have reported some work on the use of NFC for IM drive systems. In [36] the authors presented a speed control system for the induction motor drive based on the ANFIS (adaptive network-based fuzzy inference system) controller, that is, a sophisticated neuro-fuzzy controller. This ANFIS controller acts as a feed forward controller that provides the plant with the proper control input and accomplish error back-propagation algorithm through the network. However, the convergence of back-propagation algorithm is slow, which could create a problem in real-time. The authors in [37] proposed an adaptive learning pulse width modulation (PWM) for a current controller which adaptively minimizes a current ripple with a constant switching frequency. This employs neuro-fuzzy computing philosophy as well as adaptive learning pattern recognition principles to overcome the problems concerning variations of the system parameters. In [38] the authors applied neuro-fuzzy logic to induction motors condition monitoring. Two neuro-fuzzy structures are conceived to learn the exact input-output relation of the fault detection process for induction motor using measured data. The first neuro-fuzzy architecture maps the residuals into two classes: a one of fixed direction residuals and another one of faults belonging to velocity sensor. The second adaptive neuro-fuzzy network is able to provide updated membership functions of the sets of fixed oriented residuals that better describe the fault diagnosis map. However, the complexity and the computation of the algorithm are high because of the two neuro-fuzzy networks.

## 1.4 Motivation

As mentioned earlier, an induction motor is difficult to control due to its nonlinear time-varying nature. Although indirect field orientation control method has been verified extremely successful in the high performance variable speed control of induction motors, researchers are still keeping working in this area in order to enhance the performance of this method [9]. In the FOC approach, state variables are difficult to measure. Particularly, there is no direct access to the rotor to measure the d and q axes components of the rotor current. Also, there always exists measuring error in the hall-effect current sensors, even if it is accessible. Moreover, variation of rotor resistance due to temperature change and saturation of inductances make the IM system more uncertain and more difficult to control to achieve high performance criteria. Therefore, a suitable speed control system for induction motors may be required to deal with a great quantity of state variables and the non-linearities in the system. As mentioned in the literature search, the intelligent controller can be utilized to handle such nonlinearities of IM as compared to conventional PI and adaptive controller.

As an intelligent controller, a neuro-fuzzy control (NFC) scheme is considered in this work for speed control of IM since the NFC combined the advantages of FLC and ANN. Researchers have reported some work on the application of NFC for IM drive. However, the reported works did not investigate the performance of the drive over a wide speed range due to either the absence of a flux control algorithm or the absence of a tuning algorithm [33-39]. Moreover, the design approach of NFC in the

present work is different as compared to the published work in terms of selections of membership functions, fuzzy rules and tuning methods. The presented work in this thesis can be divided as:

1. Investigate the theory of the indirect field orientation control system and neuro-fuzzy control method.
2. Design an efficient neuro-fuzzy logic based speed controller for IM drive, which is capable of handling high performance motor drive and needs little trial and error for different hp induction motors.
3. Design a model reference adaptive flux (MRAF) observer, which provides effective flux regulation for FOC-IM.
4. Simulate the proposed MRAF observer based neuro-fuzzy speed controller for IM drive. Investigate the proposed neuro-fuzzy based speed controller for IM drive at different operating conditions in simulations.
5. Compare the performance of proposed neuro-fuzzy controller with a conventional PI controller and fuzzy logic controller for IM, respectively, to prove the superiority of the proposed NFC.

## 1.5 Thesis Organization

This thesis is composed of six chapters. The first chapter aims to clarify the motivation of this dissertation.

Chapter 2 introduces indirect field orientation control (FOC) of voltage source inverter (VSI) fed based induction motors. Following introduction to principles and equations of IM, indirect FOC of IM is presented and discussed. A current control method based on VSI is also presented.

Chapter 3 presents a neuro-fuzzy speed controller for FOC-IM. The detailed design of NFC and its tuning algorithm is presented. The introduction to a FLC and ANN controller is also presented in this chapter.

Chapter 4 shows the simulation results of the proposed neuro-fuzzy controller based FOC-IM drive system. The performances of the proposed NFC based IM drive are compared with PI and fuzzy logic controller.

Chapter 5 presents a model reference adaptive flux (MRAF) observer for FOC-IM. The progress on experimental implementation of the proposed drive is also reported in this chapter.

Chapter 6 provides conclusions and recommendations for future works.

## Chapter 2

# Closed Loop Field Orientation Control of Induction Motors

Induction motors, particularly the squirrel cage IMs, are probably one of the most popular motor drive systems due to their inherent advantages, such as simple structure, lower maintenance requirements, high efficiency and low cost. However, for high performance applications, their control task is very complicated and remains a challenging problem by the fact that induction motors are subject to significant nonlinearities and the parameters are of great uncertainty. Field orientation control (FOC), which is also called vector control, decouples the flux and torque control in an induction motor drive, which is similar to a separately excited dc motor. Thus, the high performance control of induction motors is theoretically feasible.

## 2.1 Coordinate Transformations

In a-b-c axis frame the machine parameters are dependent on the rotor position. In order to simplify the mathematical model of an IM drive, the  $abc \leftrightarrow dq$  axis transformation theory is utilized to provide an alternate idea to formulate dynamic modeling of an induction motor. This theory transforms traditional three axis frame into two axis frame, in other words, a-b-c axis frame is mapped to d-q axis: the direct axis, d, and the quadrature axis, q. Basically, there are three different reference frames using for dynamic modeling of an IM, which are stator reference frame, rotor and excitation (synchronous) reference frame.

In this thesis,  $d^s$  and  $q^s$  denote the d-q axes of stator reference frame, while  $d^e$  and  $q^e$  are used for excitation reference frame. Fig.2.1 shows the relationship among a-b-c axis frame, stator reference frame and excitation reference frame. Since coordinate transformations for current, voltage and flux are similar, only the instance of current is presented as follows.

The instantaneous value of the actual phase currents is given by [4]

$$\begin{aligned} i_s^s &= i_{as} \left[ \cos(0^\circ) + j \sin(0^\circ) \right] \\ &+ i_{bs} \left[ \cos(120^\circ) + j \sin(120^\circ) \right] \\ &+ i_{cs} \left[ \cos(240^\circ) + j \sin(240^\circ) \right] \\ &= i_{as} - \frac{1}{2} i_{bs} - \frac{1}{2} i_{cs} + j \left( \frac{\sqrt{3}}{2} i_{bs} - \frac{\sqrt{3}}{2} i_{cs} \right) \\ &= i_{ds}^s + j i_{qs}^s \end{aligned} \tag{2.1}$$

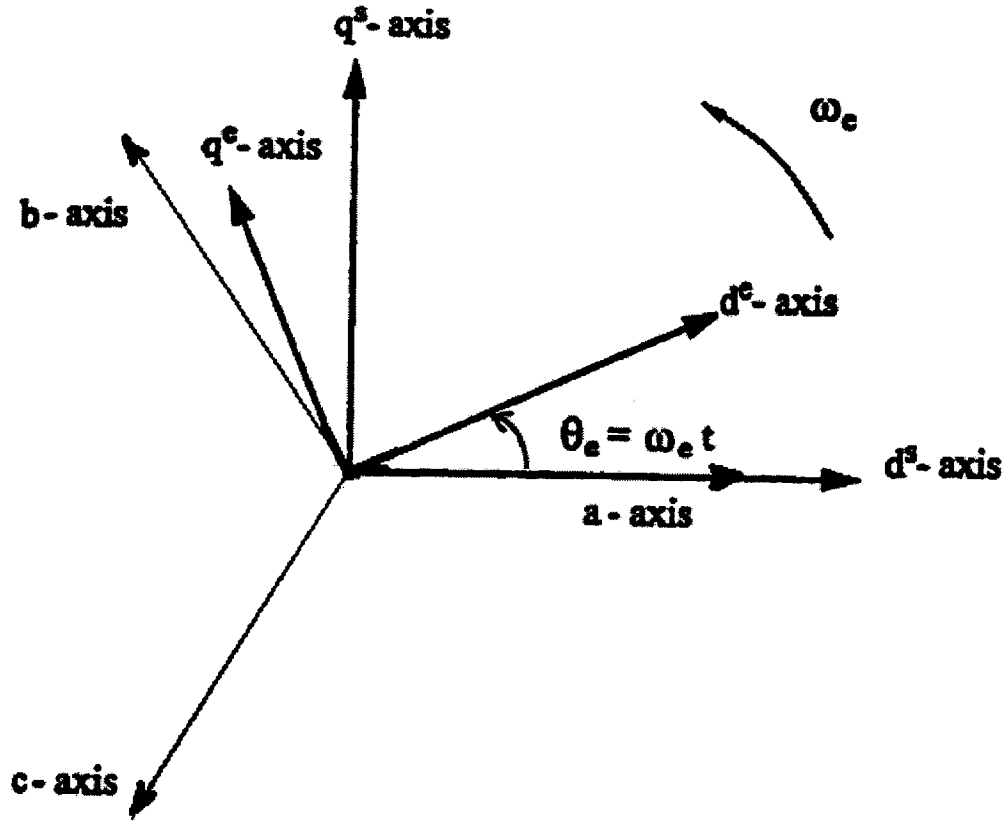


Fig.2.1: Relative positions of a-b-c, stator and excitation reference frame.

where  $i_s^s$  is the vector of stator current in the stator reference frame,  $i_{ds}^s$  and  $i_{qs}^s$  are components of the vector of stator current in the stator reference frame,  $i_{as}$ ,  $i_{bs}$  and  $i_{cs}$  are stator phase currents.

Hence,

$$\begin{bmatrix} i_{ds}^s \\ i_{qs}^s \end{bmatrix} = \begin{bmatrix} 1 & -\frac{1}{2} & -\frac{1}{2} \\ 0 & \frac{\sqrt{3}}{2} & \frac{\sqrt{3}}{2} \end{bmatrix} \begin{bmatrix} i_{as} \\ i_{bs} \\ i_{cs} \end{bmatrix} \quad (2.2)$$



Assuming a three-phase balanced supply is used, and a symmetrical three-phase motor is considered, i.e.,

$$i_{as} + i_{bs} + i_{cs} = 0 \quad (2.3)$$

Equation (2.1) can be expanded as

$$\begin{bmatrix} i_{ds}^s \\ i_{qs}^s \\ 0 \end{bmatrix} = \begin{bmatrix} 1 & -\frac{1}{2} & -\frac{1}{2} \\ 0 & \frac{\sqrt{3}}{2} & \frac{\sqrt{3}}{2} \\ 1 & 1 & 1 \end{bmatrix} \begin{bmatrix} i_{as} \\ i_{bs} \\ i_{cs} \end{bmatrix} \quad (2.4)$$

Conversely, dq-abc transformation can be derived as

$$\begin{bmatrix} i_{as} \\ i_{bs} \\ i_{cs} \end{bmatrix} = \begin{bmatrix} \frac{2}{3} & 0 \\ -\frac{1}{3} & \frac{1}{\sqrt{3}} \\ -\frac{1}{3} & -\frac{1}{\sqrt{3}} \end{bmatrix} \begin{bmatrix} i_{ds}^s \\ i_{qs}^s \end{bmatrix} \quad (2.5)$$

In contrast with stationary stator frame, excitation reference frame rotates with the same angular velocity  $\omega$  and the same direction as the stator magnetomotive force (mmf). The transformation  $d^s q^s \rightarrow d^e q^e$  from the stator reference frame to the excitation frame can be expressed as

$$\begin{bmatrix} i_{ds}^e \\ i_{qs}^e \end{bmatrix} = \begin{bmatrix} \cos(\omega t) & \sin(\omega t) \\ -\sin(\omega t) & \cos(\omega t) \end{bmatrix} \begin{bmatrix} i_{ds}^s \\ i_{qs}^s \end{bmatrix} \quad (2.6)$$

where  $i_{ds}^e$  and  $i_{qs}^e$  are components of the vector of stator current in the excitation reference frame. The inverse,  $d^e q^e \rightarrow d^s q^s$  transformation is given by

$$\begin{bmatrix} i_{ds}^s \\ i_{qs}^s \end{bmatrix} = \begin{bmatrix} \cos(\omega t) & -\sin(\omega t) \\ \sin(\omega t) & \cos(\omega t) \end{bmatrix} \begin{bmatrix} i_{ds}^e \\ i_{qs}^e \end{bmatrix} \quad (2.7)$$

## 2.2 Mathematical Model of IM

The dynamic equivalent circuit of induction motor is shown in Fig.2.2. The voltage equations of an IM can be written as [4]

$$v_s^s = R_s i_s^s + p \lambda_s^s \quad (2.8)$$

$$v_r^s = R_r i_r^s + (p - j\omega_r) \lambda_r^s \quad (2.9)$$

where  $v_s^s$  and  $i_r^s$  are vectors of stator and rotor voltages in the stator reference frame, respectively,  $R_s$  and  $R_r$  are stator and rotor resistances, respectively,  $\lambda_s^s$  and  $\lambda_r^s$  are vectors of stator and rotor flux in the stator reference frame, respectively,  $\omega_r$  is the rotor speed and  $p$  is the differential operator. Based on the mathematical model shown in equations (2.8)-(2.9), the equivalent circuit of an IM is shown in Fig 2.2. The flux vectors  $\lambda_s^s$  and  $\lambda_r^s$  can be expressed in terms of current vectors  $i_s^s$  and  $i_r^s$  and the motor inductances as

$$\begin{bmatrix} \lambda_s^s \\ \lambda_r^s \end{bmatrix} = \begin{bmatrix} L_s & L_m \\ L_m & L_r \end{bmatrix} \begin{bmatrix} i_s^s \\ i_r^s \end{bmatrix} \quad (2.10)$$

where  $L_s$ ,  $L_r$  and  $L_m$  are self inductance of stator, self inductance of rotor and mutual inductance, respectively. Substituting equation (2.10) in equations (2.8) and (2.9), the voltage equation of the IM can be obtained as

$$\begin{bmatrix} v_s^s \\ v_r^s \end{bmatrix} = \begin{bmatrix} R_s + pL_s & pL_m \\ (p - j\omega_r)L_m & R_r + (p - j\omega_r)L_r \end{bmatrix} \begin{bmatrix} i_s^s \\ i_r^s \end{bmatrix} \quad (2.11)$$

Resolving vectors in equation (2.11) into their d-q components, the voltage equation of the motor can be written as

$$\begin{bmatrix} v_{ds}^s \\ v_{qs}^s \\ v_{dr}^s \\ v_{qr}^s \end{bmatrix} = \begin{bmatrix} R_s + pL_s & 0 & pL_m & 0 \\ 0 & R_s + pL_s & 0 & pL_m \\ pL_m & \omega_r L_m & R_r + pL_r & \omega_r L_r \\ -\omega_r L_m & pL_m & -\omega_r L_r & R_r + pL_r \end{bmatrix} \begin{bmatrix} i_{ds}^s \\ i_{qs}^s \\ i_{dr}^s \\ i_{qr}^s \end{bmatrix} \quad (2.12)$$

where  $v_{ds}^s$ ,  $v_{qs}^s$ ,  $v_{dr}^s$  and  $v_{qr}^s$  are d-q axis components of the stator and rotor voltages in the stator reference frame, respectively,  $i_{dr}^s$  and  $i_{qr}^s$  are d-q axis components of the

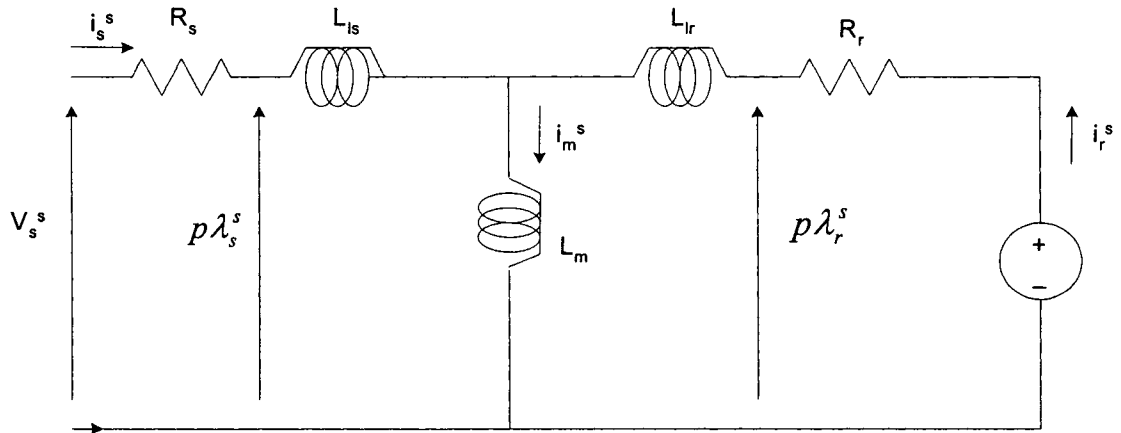


Figure 2.2: Dynamic equivalent circuit of induction motor

rotor current in the stator reference frame, respectively. Also, the voltage and current equations of the IM in the excitation reference frame can be derived in the same way as

$$\begin{bmatrix} v_{ds}^e \\ v_{qs}^e \\ v_{dr}^e \\ v_{qr}^e \end{bmatrix} = \begin{bmatrix} R_s + pL_s & -\omega L_m & pL_m & -\omega_{sl}L_m \\ \omega L_s & R_s + pL_s & \omega_{sl}L_m & pL_m \\ pL_m & -\omega_{sl}L_m & R_r + pL_r & -\omega_{sl}L_r \\ \omega_{sl}L_m & pL_m & \omega_{sl}L_r & pL_r \end{bmatrix} \begin{bmatrix} i_{ds}^e \\ i_{qs}^e \\ i_{dr}^e \\ i_{qr}^e \end{bmatrix} \quad (2.13)$$

where,  $v_{ds}^e$ ,  $v_{qs}^e$ ,  $v_{dr}^e$  and  $v_{qr}^e$  are d-q axis components of the stator and rotor voltages in the excitation reference frame, respectively,  $i_{dr}^e$  and  $i_{qr}^e$  are d-q axis components of the rotor current in the excitation reference frame, respectively,  $\omega_{sl}$  is the slip speed of a motor. The rotor voltage vector is normally assumed as zero because of the shorted rotor winding, i.e.,  $v_{dr}^e = v_{qr}^e = 0$ .

The torque developed by the motor in stator reference frame is given by [5]

$$T = \frac{3P}{2} L_m (i_{qs}^s i_{dr}^s - i_{ds}^s i_{qr}^s) \quad (2.14)$$

where  $P$  is the number of pole-pairs. And the torque equation in the excitation reference frame is similar to that in the stator frame, which is given by

$$T = \frac{3P}{2} L_m (i_{qs}^e i_{dr}^e - i_{ds}^e i_{qr}^e) \quad (2.15)$$

Equations (2.12), (2.14) and (2.13), (2.15) represent the mathematical dynamic model of an induction motor in stator and excitation reference frame, respectively.

## 2.3 Field Orientation Control

The instantaneous electromagnetic torque equation using excitation reference frame equation (2.15) can also be expressed as

$$T = \frac{3P}{2} \frac{L_m}{L_r} (i_{qs}^e \lambda_{dr}^e - i_{ds}^e \lambda_{qr}^e) \quad (2.16)$$

where

$$\lambda_{dr}^e = L_r i_{dr}^e + L_m i_{ds}^e \quad (2.17)$$

and

$$\lambda_{qr}^e = L_r i_{qr}^e + L_m i_{qs}^e \quad (2.18)$$

where  $\lambda_{dr}^e$  and  $\lambda_{qr}^e$  are d-q axis components of the rotor flux linkage in the excitation reference frame. The key feature of the field-oriented control is to keep the magnetizing current at constant rated value, which is expressed using excitation reference frame as

$$\lambda_{qr}^e = 0 \quad (2.19)$$

$$\lambda_{dr}^e = \text{constant} \quad (2.20)$$

Substituting equations (2.19) and (2.20) in the torque equations (2.16)

$$i_{qs}^e = \frac{T}{K_T \lambda_{dr}^e} \quad (2.21)$$

or

$$T = K_T \lambda_{dr}^e i_{qs}^e \quad (2.22)$$

where  $K_r = \frac{3P}{2} \frac{L_m}{L_r}$ . Also, the current component  $i_{ds}^e$  corresponding to a given reference rotor flux  $\lambda_{dr}^e$  can be given as [4]

$$i_{ds}^e = \frac{1 + \tau_r p}{L_m} \lambda_{dr}^e \quad (2.23)$$

where  $\tau_r = \frac{L_r}{R_r}$  is the rotor time constant. The electrical angle  $\theta_e$ , which is required in the process of coordinate transformation  $d^e q^e \rightarrow abc$ , is given by

$$\theta_e = \int (\omega_{sl} + P\omega_r) dt \quad (2.24)$$

and

$$\omega_{sl} = \frac{L_m}{\tau_r} \frac{i_{qs}^e}{\lambda_r} \quad (2.25)$$

where  $\omega_{sl}$  is the slip speed of the motor in electrical rad/sec, and  $\omega_r$  is the mechanical speed of the motor. Equation (2.22) represents an induction motor as a linear current-to-torque converter. Equation (2.23) indicates that  $i_{ds}^e$  controls the rotor flux  $\lambda_r$ . Thus, the rotor torque and flux can be controlled separately through  $i_{qs}$  and  $i_{ds}$ , respectively, which is analogous to a separately-excited dc motor. There are two types of FOC-IM drive such as direct and indirect FOCs. In a direct FOC, the angular position  $\theta_e$  is measured directly using air gap flux sensors, whereas the indirect FOC approach is based on the calculation of the slip speed  $\omega_{sl}$  to obtain the angular position  $\theta_e$ . In a popular indirect FOC-IM scheme, the torque reference  $T_e^*$  is generated from the speed error via the speed controller, while the flux reference  $\lambda_r^*$  is kept constant in

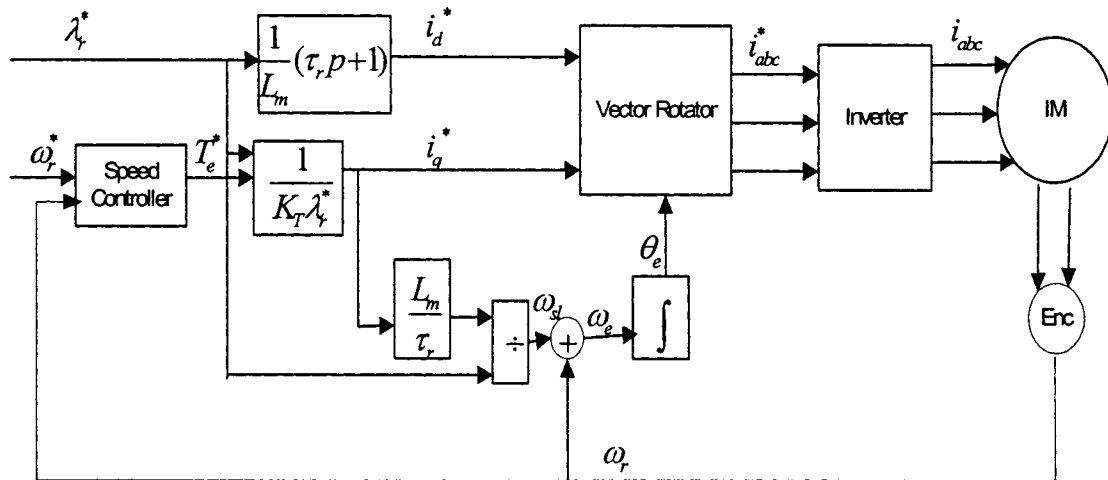


Figure 2.3: Closed loop indirect FOC scheme

each operating period. A typical closed loop indirect FOC scheme for an IM is shown in Fig.2.3.

## 2.4 Voltage Source Inverter

Three phase inverters play a very important role in variable speed IM drive systems [10, 44-46]. They supply voltages and currents of adjustable frequency and magnitude to the IM stator. Voltage source inverters (VSI) constructed with BJT's are often used in drive industry rather than current source inverters, due to the fast transient response. A diagram of the power circuit of a three-phase VSI is shown in Fig 2.4. The circuit has bridge topology with three branches (phases), each consisting of two power switches and two freewheeling diodes. An uncontrolled, diode-based rectifier is used to supply the inverter, via a dc. link which contains an LC filter. Three-phase power is supplied to the induction motor via the middle of each branch of switches, as illustrated in Fig 2.4. The power switches in a given branch are

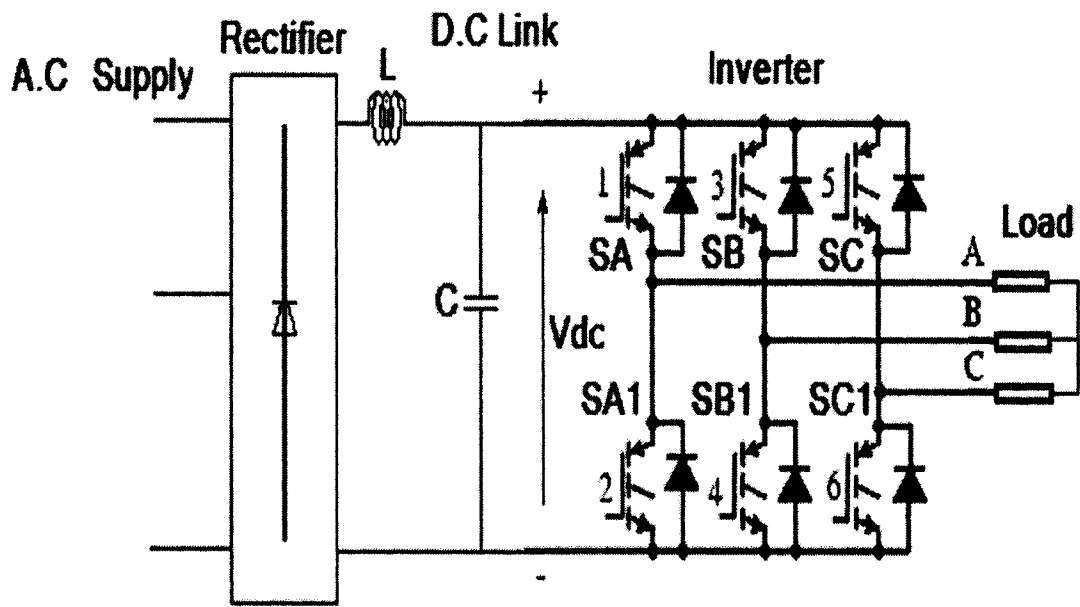


Fig 2.4: Circuit diagram of a three-phase VSI

forbidden to be in the ON-state simultaneously. On the other hand, the status that both the switches are in the OFF-state should also be avoided; otherwise the potential of the corresponding output terminal is unknown to the control system of the inverter. Therefore, a VSI is working in such a way that, in a given branch (phase), one switch must be ON and the other must be OFF; in other words, only two combinations of states of the switches in each branch are allowed. Assuming a switching (logic) variable is assigned to each phase of the inverter, eight logic states are composed for the whole power circuit as shown in Table 2.1.



State (abc) <sub>2</sub>	Phase A (LA)		Phase B (LB)		Phase C (LC)		Operating Modes	Voltage Phaseor
	SA	SA1	SB	SB1	SC	SC1		
0	0	1	0	1	0	1	Freewheeling	V0
1	1	0	0	1	0	1	Active	V1
2	0	1	1	0	0	1	Active	V2
3	1	0	1	0	0	1	Active	V3
4	0	1	0	1	1	0	Active	V4
5	1	0	0	1	1	0	Active	V5
6	0	1	1	0	1	0	Active	V6
7	1	0	1	0	1	0	Freewheeling	V7

Table 2.1: Conduction modes of the VSI under current control

The switching variables are defined as

$$LA= 0 \text{ if SA is OFF and SA1 is ON} \quad (2.26)$$

$$1 \text{ if SA is ON and SA1 is OFF}$$

$$LB= 0 \text{ if SB is OFF and SB1 is ON} \quad (2.27)$$

$$1 \text{ if SB is ON and SB1 is OFF}$$

$$LC= 0 \text{ if SC is OFF and SC1 is ON} \quad (2.28)$$

$$1 \text{ if SC is ON and SC1 is OFF}$$

The line-to-neutral voltages of the inverter are given by

$$V_a = \frac{V_{dc}}{3}(2LA - LB - LC) \quad (2.29)$$

$$V_b = \frac{V_{dc}}{3}(2LB - LC - LA) \quad (2.30)$$

$$V_c = \frac{V_{dc}}{3}(2LC - LA - LB) \quad (2.31)$$

Equations (2.29)-(2.31) indicate that line-to-neutral voltage can assume any one of five values at each logic states:  $-2/3V_{dc}$ ,  $-1/3V_{dc}$ ,  $0$ ,  $1/3V_{dc}$ ,  $2/3V_{dc}$ . Performing the abc-dq transformation:

$$\begin{bmatrix} u_d \\ u_q \end{bmatrix} = \begin{bmatrix} 1 & -\frac{1}{2} & -\frac{1}{2} \\ 0 & \frac{\sqrt{3}}{2} & -\frac{\sqrt{3}}{2} \end{bmatrix} \begin{bmatrix} u_a \\ u_b \\ u_c \end{bmatrix} \quad (2.32)$$

output voltages can be represented as space vectors in the stator reference frame, each vector corresponding to a given state of the inverter. Fig 2.5 illustrates the space vector diagram of line-to-neutral voltages of a VSI. From states 1 to 6, the magnitude of the vector in stator reference frame is equal to  $U_{dc}$  and the phase angle is  $0, 60, \dots, 300$ , respectively, while in states 0 and 7, the stator voltage vectors are zeros.

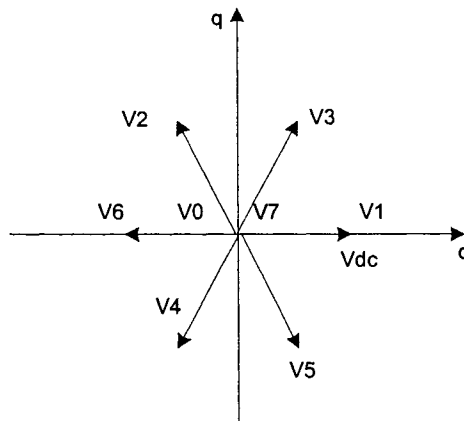


Fig.2.5: Space vectors of output voltages of a VSI

## 2.5 Speed Controller

The speed controller processes the error between command and actual speeds and generates the command torque. The small change in speed  $\Delta\omega_r$  produces a corresponding change in torque  $\Delta T_e$  and taking the load torque  $T_L$  as a constant. In a traditional PI controller based IM drive, the control algorithm can be written as,

$$T_e^* = K_p \Delta\omega_r + K_i \int_0^t \Delta\omega_r dt \quad (2.33)$$

where  $K_p$  is the proportional constant,  $K_i$  is the integral constant and  $\Delta\omega_r = \omega_r^* - \omega_r$  is the speed error between the command speed  $\omega_r^*$  and the actual motor speed  $\omega_r$ . In Laplace domain, equation (2.33) can be written as,

$$T_e^* = \left(K_p + \frac{K_i}{s}\right) \Delta\omega_r(s) \quad (2.34)$$

Substituting for  $s = \frac{2}{T_s} \left(\frac{1-z^{-1}}{1+z^{-1}}\right)$  in equation (2.34) where  $z^{-1}$  represents one sample delay and  $T_s$  is the sampling period, or by differentiating equation (2.33) and then replacing the continuous terms by their finite differences, the discrete form of the PI algorithm can be written as,

$$T^*(k) = T^*(k-1) + K_p [\Delta\omega_r(k) - \Delta\omega_r(k-1)] + K_i T_s \Delta\omega_r(k) \quad (2.35)$$

where  $T^*(k)$  is the present sample of command torque,  $T^*(k-1)$  is the past sample of command torque,  $\Delta\omega_r(k)$  is the present sample of speed error and  $\Delta\omega_r(k-1)$  is the past sample of speed error. Equation (2.35) can be easily implemented using a DSP if the values of  $K_p$ ,  $K_i$ ,  $T_s$  and the command speed are chosen properly.

## 2.6 Hysteretic current control

Hysteretic current control is one of the most effective and simple control methods. A typical three-phase hysteretic current control fed VSI is shown in Fig 2.6. Current error signals  $\Delta i_a$ ,  $\Delta i_b$ , and  $\Delta i_c$  are generated by comparing the output currents of the inverter and the reference current  $i_a^*$ ,  $i_b^*$  and  $i_c^*$ . Switching signals a, b and c fed to VSI are generated by operating current error signals  $\Delta i_a$ ,  $\Delta i_b$ , and  $\Delta i_c$  in the hysteretic current controller. Fig 2.7 presents the input-output characteristic of one phase in hysteretic current controller. The tolerance bandwidth for the current controller is denoted by  $h$  shown in Fig 2.7. In each operating loop, if the current error  $\Delta i$  is greater than  $h/2$ , the switching variable is set to 1; conversely, if the current error  $\Delta i$  is less than  $h/2$ , the switching variable is set to 0; otherwise, the switching variable keeps the same status of last loop. It's been obvious that the bandwidth  $h$  affects the switching frequency of the inverter. The narrower is the  $h$ , the more frequent switching operates and the higher quality of output of the inverter. In a typical VSI fed FOC-IM, the three-phase current command  $i_a^*$ ,  $i_b^*$  and  $i_c^*$  are compared with the actual current  $i_a$ ,  $i_b$  and  $i_c$  to generate PWM signals, which will fire the three-phase voltage source inverter to produce the actual voltages to the motor.

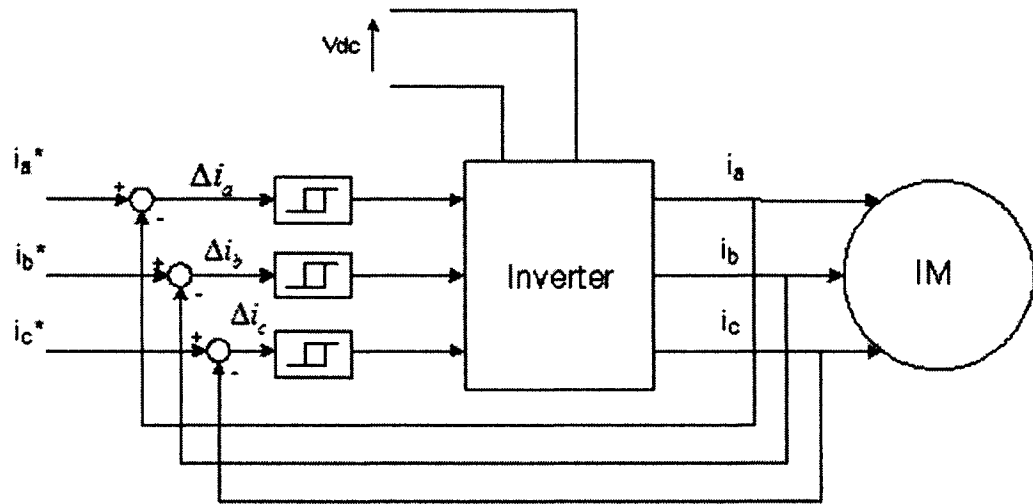


Fig 2.6: Block diagram of a current-controlled VSI for IM drive

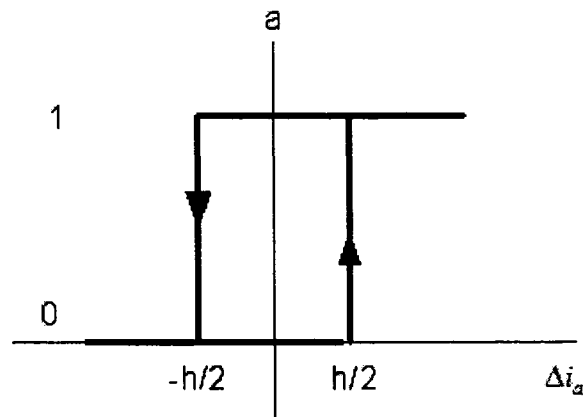


Fig 2.7: Input-output characteristic of a hysteresis current controller

## 2.7 Summary

In this chapter, the transformation between a-b-c and d-q frame of a phasor quantify is discussed in detail. The step-by-step derivation of d-q axis mathematical model of IM is presented. The derivation of FOC theory based on d-q axis IM model is discussed. The circuit scheme and operational process of VSI is presented in detail. A traditional PI based speed controller for FOC-IM drive is discussed. A hysteretic current control method is also introduced. Thus, this chapter gives a good idea about FOC of IM and the pertinent mathematical equations.

## Chapter 3

# Development of Neuro-Fuzzy Controller

Artificial intelligence (AI) has been applied in industrial applications since the early 1960s [49]. In the beginning, AI was used mostly in the area of expert knowledge-based decision making for the design and monitoring of industrial products or processes [50]. Over the last two decades, researchers have applied some AI algorithms for electric motor drives. The application of AI has been enhanced with advances in computer technology and the advent of powerful personal computers. Thus, many approaches of intelligence have been realized. Among different intelligent computational algorithm based control approaches, fuzzy logic control (FLC), artificial neural network (ANN) and neuro-fuzzy control (NFC) are the most popular intelligent control methods. In the last two decades, fuzzy logic received a high boost in industry, and fuzzy logic control (FLC) gradually became a significant approach in industrial control field [49]. However, there are several inconveniences in the approach of traditional/pure fuzzy logic control:

1. Difficulties in determination of practical fuzzy set parameters in fuzzification and/or defuzzification employed by an FLC.
2. Difficulties or inability to learn how to control the systems with a rapidly changing systems or systems performing complicated input/output mappings, and thus the controller's inability to formulate the fuzzy model of such a process.

Above reasons have motivated researchers to develop the fuzzy self-tuning models. The method of neuro-fuzzy (NF) networks is one of such approaches. The neural networks can be trained on the basis of the input/output measurements of the modeled system. A fuzzy model can be presented in the form of a special neural network and one of the training methods can be applied to model parameter tuning.

## 3.1 Fuzzy Logic Control

Fuzzy logic controller is mainly based on fuzzy logic theories introduced by Zadeh in 1965 [27]. A general fuzzy logic controller consists of three modules: fuzzy inference engine, fuzzification and defuzzification modules. Fig.3.1 shows a general block diagram of a fuzzy logic controller. Input crisp numbers are converted into fuzzy values with the fuzzification block. The fuzzy inference engine determines how the fuzzy logic operations are performed; in other words, it performs fuzzy IF-THEN rules together with knowledge base. Defuzzification block is used to combine and convert those outputs of rules to crispy values.



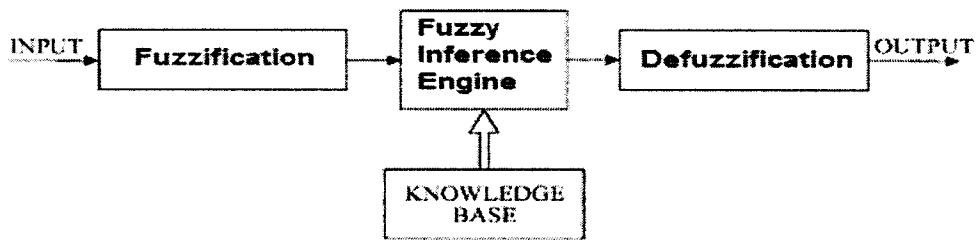


Fig. 3.1 Block diagram of fuzzy logic control

### 3.1.1 Fuzzification

Fuzzification is the process of transferring crisp input values of the FLC into fuzzy numbers through membership functions. In the practice of fuzzy numbers, many various types of membership functions such as triangular, trapezoidal, rectangular, Gaussian and sigmoid membership functions are applied. Figure 3.2 shows a system of fuzzy sets for an input with triangular membership functions. There are three membership functions which indicate the speed as slow, middle and fast, respectively. A certain crisp number is mapped by all three membership functions, thus a fuzzy number with three components is obtained. For example, the crisp number 70 (rad/s) is converted into a fuzzy number as 0.3 degree of SLOW, 0.7 degree of MIDDLE and 0 degree of FAST, as shown in Fig.3.2.

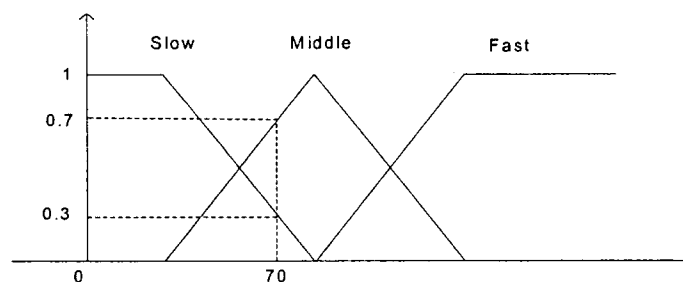


Fig.3.2: The example of membership function and fuzzification

### 3.1.2 Fuzzy Inference Engine

A fuzzy inference engine consists of a set of expert rules, which reflect the knowledge base and reasoning structure of the solution of any problem. A typical fuzzy rule can be composed as

$$\begin{aligned} \text{IF } A \text{ is } A1 \text{ AND } B \text{ is } B1 \text{ OR } C \text{ is } C1 \\ \text{THEN } U \text{ is } U1 \end{aligned} \quad (3.1)$$

where A, B, C and U are fuzzy variables, A1, B1, C1 and U1 are fuzzy linguistic values (membership functions), “AND”, ”OR” are connectives of the rules. The above rule is known as Mamdani type rule, whose antecedent and consequent parts are both expressed using linguistic labels. Another form is Sugeno rules in which the consequent part is expressed as an analytical expression or equation. Fig. 3.3 shows an example of expressing a set of rules in FLC.

### 3.1.3 Defuzzification

The output decision of a fuzzy logic controller is a fuzzy value and is represented by a membership function. Because only the crisp number can be utilized in industry systems, the control inference must be defuzzified for practical purposes. Several methods are available for defuzzification of a fuzzy control inference such as centroid method, mean of maxima and threshold methods. An example of defuzzification is also shown in Fig. 3.3, which demonstrates max-min inferencing and centroid defuzzification method. In this case, rule outputs are combined, and the gravity of the combined shape is indicated as the defuzzification result.

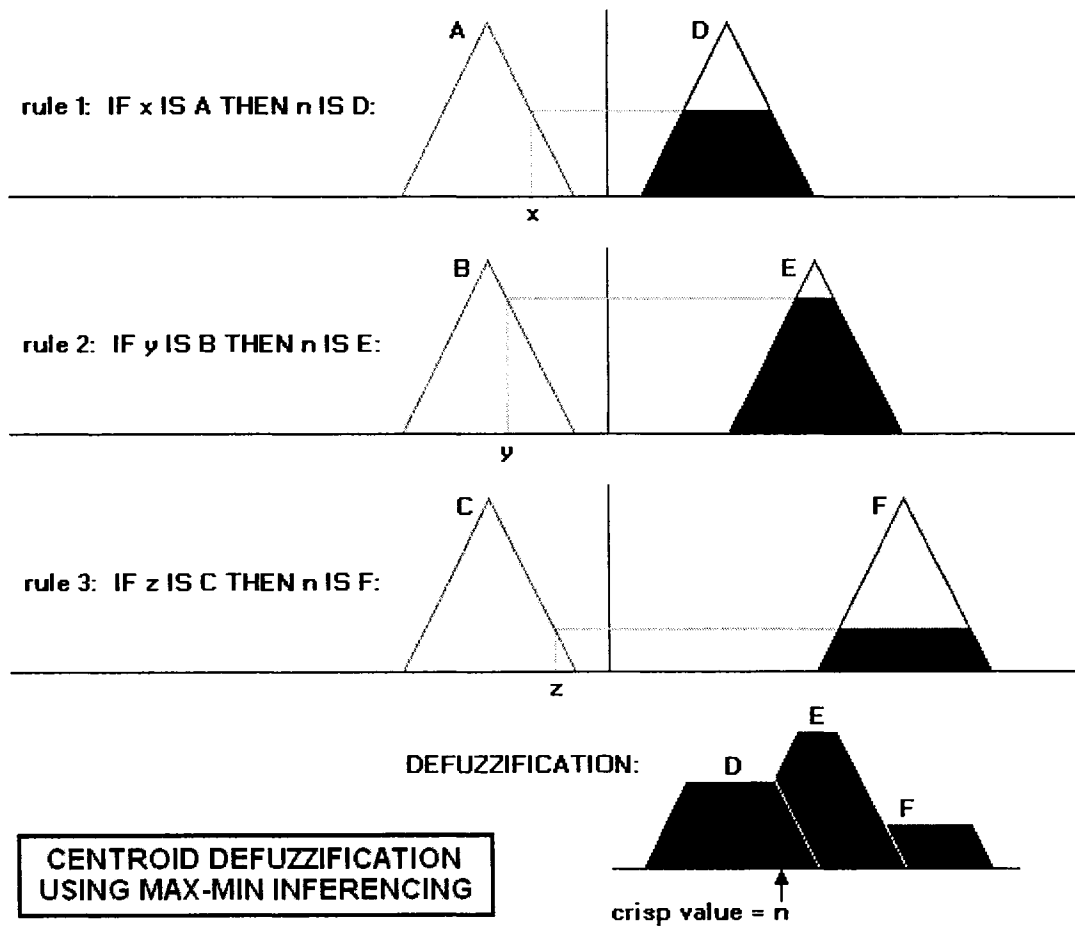


Fig.3.3: The example of expressing a set of rules and defuzzification.

## 3.2 Neural Network

The fundamental processing element of a neural network is a neuron, which receives input from some other units, or perhaps from an external source [50]. Each input of a neuron has an associated weight  $w$ , which can be modified for

tuning/learning reason. Then an activation function  $f$  is applied to the weighted sum of its inputs:

$$y_i = f\left(\sum_j w_{ij} y_j\right) \quad (3.2)$$

The activation functions may be exponential, sigmoid, and etc. Figure 3.4 shows a typical structure of an artificial neural network. It consists of three layers, which are input layer, hidden layer and output layer. The layer of input neurons receive the data either from input files or electronic sensors in real-time applications. The hidden layer contains many of the neurons in various interconnected structures. The output layer sends information directly to the outside world. There are a number of approaches for training neural networks. However, they are mostly classified as two modes such as supervised/offline learning and unsupervised/online learning. In offline learning,

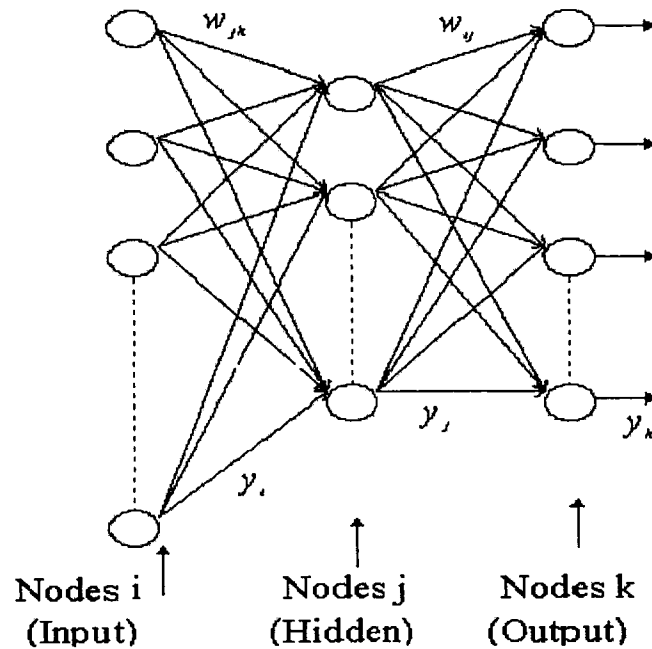


Fig 3.4: The example of a typical structure of neural network

the purpose of a neural network is to change its weights according to the inputs and outputs samples. After a network has established its input/output mapping with a defined minimum error value, the training task has been completed. An important factor of the offline training is that the training set should be comprehensive and cover all the practical areas of applications of the network. Obviously, offline training method based ANN isn't competent for the control of IM drives which possesses a great quantity of uncertainties. In an online learning based ANN, weights between neurons are updated in each operating cycle without any inputs/outputs samples.

The most popular algorithm for adjusting weights during the training phase is called back-propagation method [51]. Since the initial configuration of ANN is arbitrary, the result of presenting a pattern to the ANN is likely to produce incorrect output. The errors for all input patterns are propagated backwards, from the output layer towards the input layer. The corrections to the weights are selected to minimize the residual error between actual and desired outputs. The algorithm can be viewed as a generalized least squares technique applied to multiplayer perceptron. Generally, a learning equation for a back-propagation method can be written as

$$\Delta w_{ij} = -\eta \frac{\partial E}{\partial w_{ij}} \quad (3.3)$$

where  $\eta$  is the learning rate,  $E$  is the error defined as  $E = \frac{1}{2}(y - o)^2$ , where  $y$  is the desired output and  $o$  is the actual output.

### 3.3 Design of a Specific Neuro-fuzzy Controller

As mentioned earlier in chapter 1, the FLC and ANN have their own advantages and drawbacks. In order to get the advantages from both FLC and ANN, researchers developed NFC for motor drive applications [36-43]. The proposed neuro-fuzzy controller (NFC) incorporates fuzzy logic algorithms with a five-layer artificial neural network (ANN) structure as shown in Fig.3.5. The proposed fuzzy logic algorithm is based on Sugeno method [52]. In the five-layer ANN structure the first layer represents for inputs, the second layer represents for fuzzification, the third and fourth layers represent for fuzzy rule evaluation and the fifth layer represent for defuzzification. A tuning block is utilized to adjust the parameters of only 4<sup>th</sup> layer in order to correct any deviation of control effort and decrease computational burden.

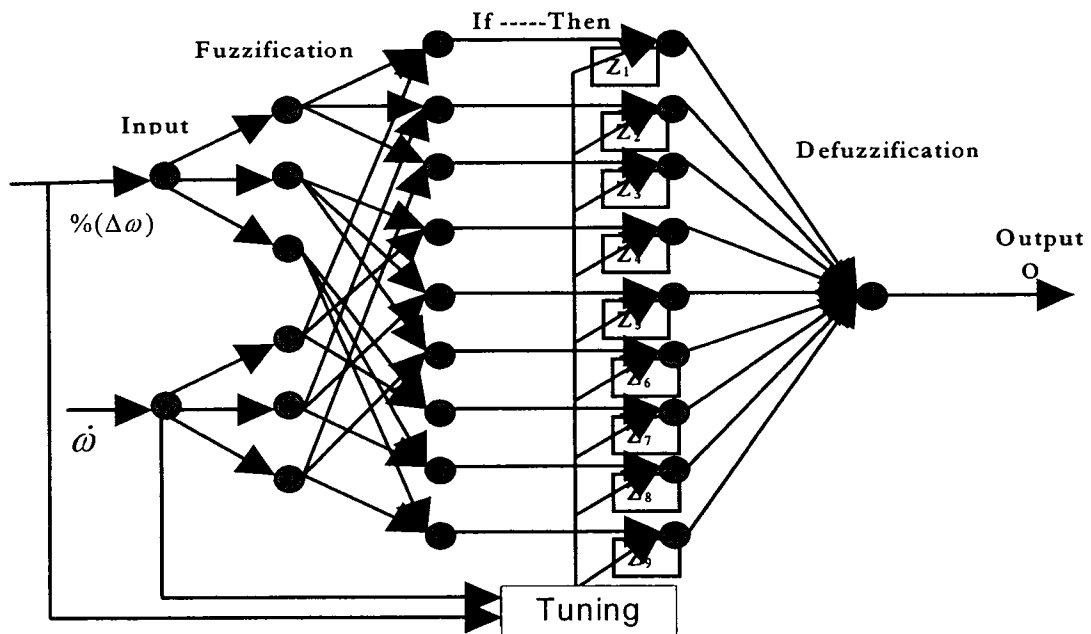


Fig 3.5: Structure of the NF controller.

### 3.3.1 Detailed Structure of NFC

The function of each layer of the proposed NFC is briefly described as follows:

*Layer I:* In this layer normalized speed error and the rate of change of actual speed are calculated. These are the inputs of the proposed NFC, which are given by,

$$O_1^I = \text{Fuzzy Input1} = \frac{\omega_r^* - \omega_r}{\omega_r^*} * 100\% \quad (3.4)$$

$$O_2^I = \text{Fuzzy Input2} = \frac{\omega_r(n) - \omega_r(n-1)}{T} * 100\% \quad (3.5)$$

where  $O_1^I$  and  $O_2^I$  are the outputs of the 1<sup>st</sup> layer for input 1 and 2, respectively, T is the sampling time,  $\omega_r^*$  is the command speed,  $\omega_r(n)$  is the present sample and  $\omega_r(n-1)$  is the previous sample of the actual speed.

*Layer II:* This is the fuzzification layer where the crisp value of each input is transformed to the fuzzy number through the membership functions. In the fuzzification process two choices of membership functions are taken for two inputs, which are shown in Fig 3.6. One choice is the three membership functions (which are mf1, mf2 and mf3) scheme as shown in Fig. 3.6(a) and the other is two membership functions (which are mf1 and mf2) scheme as shown in Fig. 3.6(b). Although more choices are available but to keep the computational burden low only these two cases are considered. Gaussian function and sigmoid function are chosen as the membership functions in this proposed NFC, which are shown in Fig. 3.6.

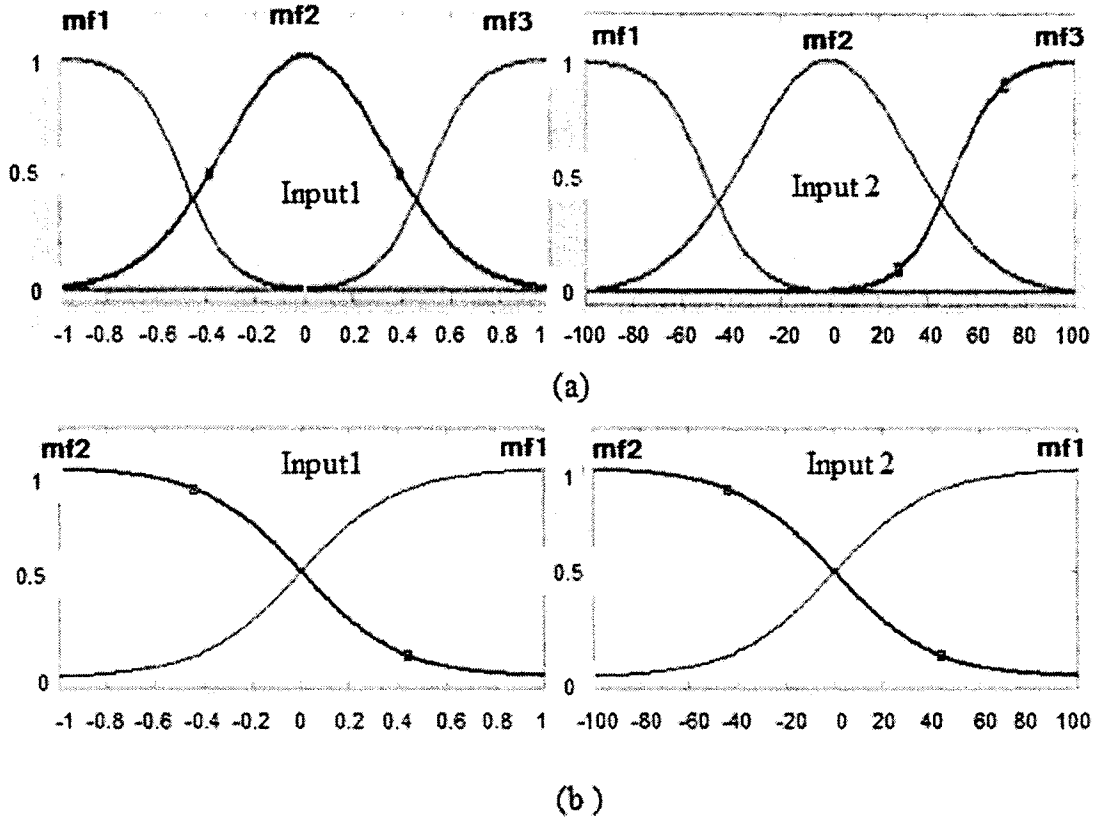


Fig 3.6: Membership functions of inputs: (a) 3 membership functions scheme, and (b) 2 membership functions scheme

The node equations for Gaussian membership function in layer II is given as,

$$O_i^{II} = e^{-\frac{0.5(x_i^{II} - c)^2}{\sigma^2}} \quad (3.6)$$

where  $O_i^{II}$  and  $x_i^{II}$  denote the output and input for i-th node in layer II, respectively,  $c$  is the center of Gaussian function, and  $\sigma$  is the curvature of Gaussian function.



*Layer III:* This is the first step of fuzzy rule evaluation. For rule evaluation in this proposed NFC the multiplication method is chosen to implement the ‘AND’ logic. Since there are two inputs with each having three membership functions, nine nodes are assigned in this layer covering all cases, while there are four nodes for the two-membership functions scheme. The node equation in layer III can be specified as,

$$O_i^{III} = \prod x_j^{III} x_k^{III} = x_i^{IV} \quad (3.7)$$

where  $O_i^{III}$  denotes the output for i-th node in layer III,  $x_j^{III}$  and  $x_k^{III}$  are components of fuzzy numbers from  $\Delta\omega$  and  $d\omega/dt$ , respectively, which denote inputs for i-th node in layer III, and  $x_i^{IV}$  denotes the input for i-th node in layer IV.

*Layer IV:* This is the final step of fuzzy rule evaluation. As mentioned earlier, Sugeno mode is adopted in this proposed NFC, which utilizes crisp numbers instead of fuzzy numbers as the rule’s results. Therefore, the computational burden is alleviated, because it doesn’t have the complicated defuzzification process that can be found in the Mamdani mode [52]. The node equation in this layer can be specified as,

$$O_i^{IV} = Z_i^{IV} x_i^{IV} = x_i^V \quad (3.8)$$

where  $x_i^{IV}$ , and  $O_i^{IV}$  denote the input and output for i-th node in layer IV, respectively,  $Z_i^{IV}$  is the adaptive weight factor for the i-th node and  $x_i^V$  denotes the input for the i-th node in layer V.

*Layer V*: This is the defuzzification layer, which is the final layer of the network. For defuzzification the center of gravity method is used to determine the output of the NFC. The node equation in this layer can be specified as,

$$O^V = \frac{\sum x_i^V}{\sum O_i^{III}} \quad (3.9)$$

where  $O^V$  is the output of layer V, which is the final output of the controller. Substituting Eqns (3.7) and (3.8) in Eqn (3.9), the output of the NFC can be rewritten as,

$$O^V = \frac{\sum Z_i^{IV} x_i^{IV}}{\sum O_i^{III}} = \frac{\sum Z_i^{IV} O_i^{III}}{\sum O_i^{III}} \quad (3.10)$$

For the proposed NFC based IM drive this control output represents the q-axis command current of the stator,  $i_q^*$  in synchronously rotating frame. This current is responsible to force the motor to follow a reference speed trajectory.

### 3.3.2 Tuning Method

Since it is almost impossible to determine desired  $i_q$  as the training data, a new method is developed to update the weight  $Z_i^{IV}$  based on the error between reference model and actual motor speed accelerations. A reference model of motor speed  $\omega_r$  and corresponding speed slope  $(d\omega_r/dt)^*$  is designed according to the specific requirements of IM drive as shown in Fig. 3.7. The corresponding equation is given by,

$$y = (1 - \exp(\frac{-(\omega)^2}{2 * 0.01^2})) * 1000 * \text{sign}(\omega) \quad (3.11)$$

where  $y$  denotes the reference speed slope  $(d\omega_r/dt)^*$ . Thus, the error for neuro-fuzzy network can be defined as the difference between desired speed slope  $(d\omega_r/dt)^*$  and actual speed slope  $d\omega_r/dt$ , which is given by

$$E = \frac{1}{2} (y - \frac{d\omega_r}{dt})^2 = \frac{1}{2} (y - O_2^I)^2 \quad (3.12)$$

The parameter  $Z_i^{IV}$  in the 4<sup>th</sup> layer is updated in order to minimize this error. Since the torque current component  $i_q$  is proportional to the acceleration  $d\omega/dt$ , the relation between  $O_2^I$  and  $O^V$  can be written as,

$$O_2^I = kO^V \quad (3.13)$$

where  $k$  is a proportionality constant. Based on Eqns. (3.10) and (3.11) the updated laws can be written as,

$$Z_i^{IV}(n) = Z_i^{IV}(n-1) - \eta' \frac{\partial E}{\partial Z_i^{IV}} = Z_i^{IV}(n-1) - \eta' \frac{\partial E}{\partial O_2^I} \frac{\partial O_2^I}{\partial Z_i^{IV}} \quad (3.14)$$

Using Eqns (3.10), (3.13) and (3.14), the self-learning algorithm is obtained as,

$$Z_i^{IV}(n) = Z_i^{IV}(n-1) + \eta (y - \frac{d\omega}{dt}) \frac{O_i^{III}}{\sum O_j^{III}} \quad (3.15)$$

where  $\eta = k * \eta'$ , is the learning rate which is set to 0.07 in this controller. The  $\eta$  can be obtained either by trial and error or self-tuning method. In this proposed NFC,  $\eta$  is

designed by trial and error method which is explained in Fig.3.8. Figure 3.8 shows simulation results of steady-state speed response, current response and torque response for different values of  $\eta$ . Three simulation result sections with different values of  $\eta$ , which are 0.07, 3 and 0.005, respectively, are put together in order to make an explicit comparison. It can be found that large IM current, torque and high speed deviation occurred in the case of large value of  $\eta$ . On the other hand, NFC with relatively small  $\eta$  cannot retain the IM speed at its reference of 180 rad./sec. constantly.

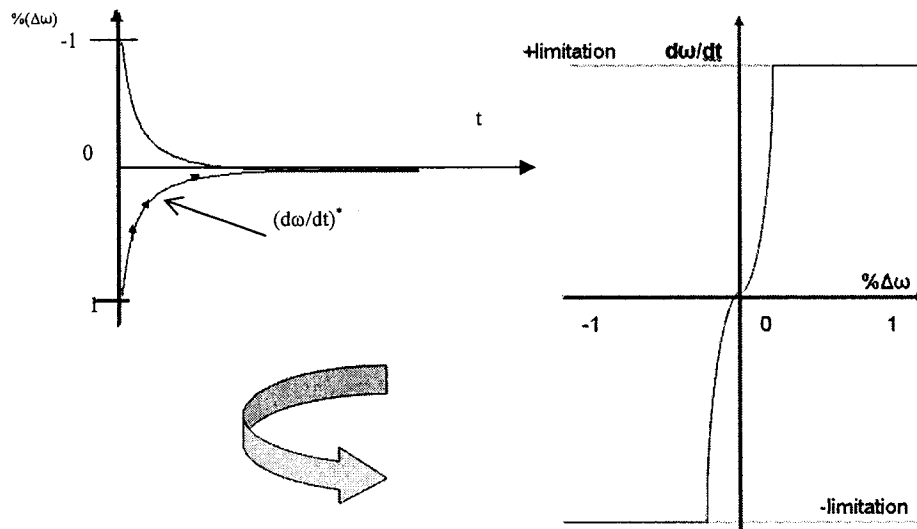
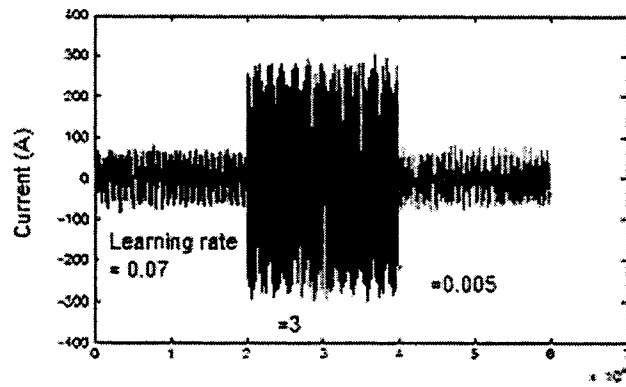
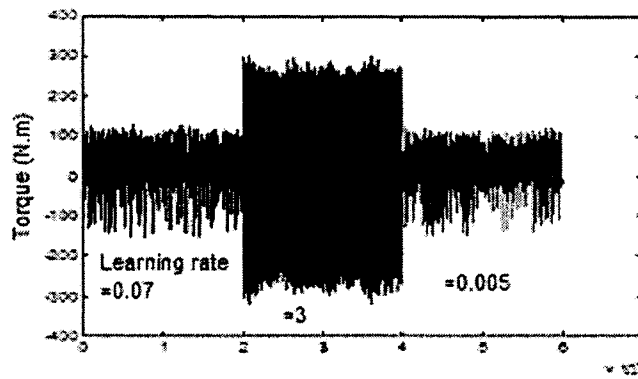


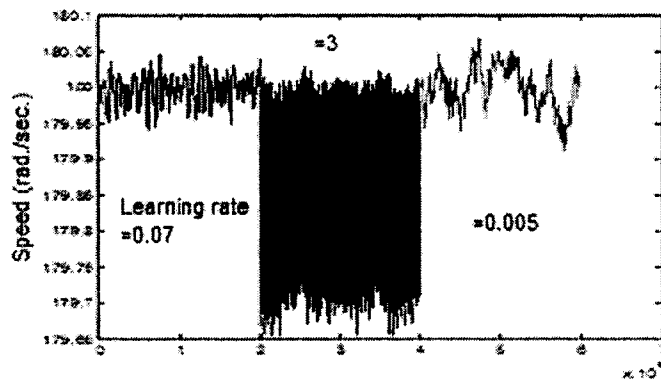
Fig.3.7: Design reference of  $d\omega/dt$ .



(a)



(b)



(c)

Fig.3.8: Comparison of current  $i_a$ , torque and steady-state speed response, respectively, under conditions of different  $\eta$  : (a) current  $i_a$ , (b) torque, and (c) speed.

# Chapter 4

## Simulation of NFC based FOC of IM Drive

A key step towards studying and testing NFC based FOC-IM is to implement the complete drive system in software simulations. The simulation of the proposed IM drive system has been carried out using MATLAB/Simulink software and power system toolbox [55].

### 4.1 Drive System

Based on the control schemes described in chapters 2 and 3, the schematic diagram of the NFC based FOC for IM drive system is shown in Fig.4.1. The rotor speed is measured and compared with the reference speed. Rotor speed error,  $\Delta\omega$  is applied to the neuro-fuzzy based speed controller, which yields reference torque  $T_e^*$ , or reference current  $i_q^*$  directly. Generally, reference flux  $\lambda_r^*$  can be generated in three ways: assigned a constant, formed from flux weakening regulation or flux controller. In this proposed IM drive, a constant is used to as the reference flux  $\lambda_r^*$ . Therefore,

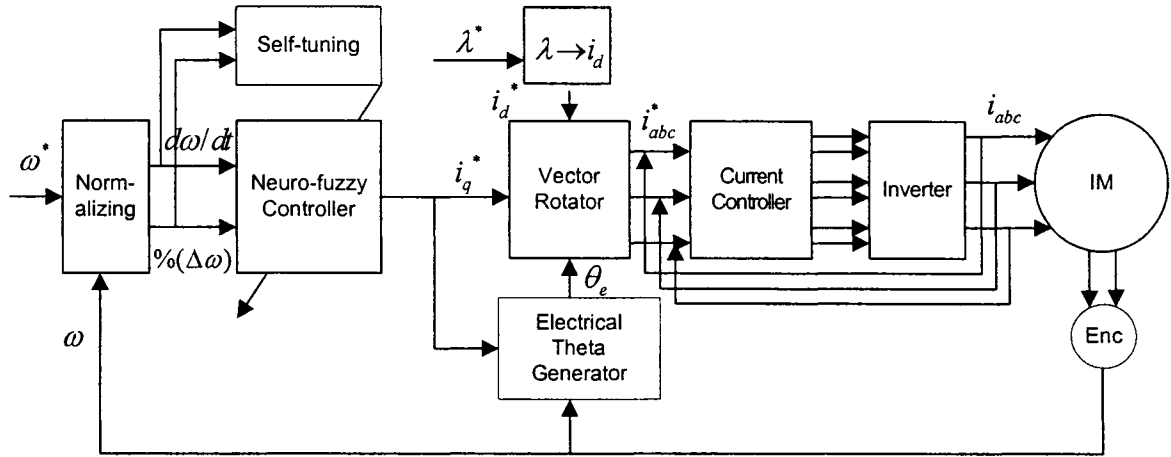


Fig 4.1: Proposed NFC based IM drive

both d-q axes reference currents  $i_q^*$  and  $i_d^*$  are obtained. Vector rotator is used to transfer currents from d-q axis to a-b-c axis components. The actual phase currents  $i_a$ ,  $i_b$  and  $i_c$ , are compared with the corresponding three-phase command currents  $i_a^*$ ,  $i_b^*$  and  $i_c^*$  and then the current errors are processed through the current controllers to generate six PWM logic signals. The three independent hysteresis regulators are used as current controllers in this work. The PWM logic signals are used to fire the switches of the three-phase voltage source inverter to produce the actual voltages to the motor.

## 4.2 Simulation Results and Discussion

In order to demonstrate the high performance of the proposed NFC, numerous simulation tests were performed under different operating conditions such as a sudden change of command speed, a sudden change of load, parameters variations, etc.

Furthermore, in order to prove the superiority of the proposed NFC, comparisons between the proposed NFC and the traditional PI controller, as well as a fuzzy logic controller (NFC), are also presented. Simulations were built on a 50 hp induction motor model indicated in the appendix and three membership functions scheme illustrated in Fig.3.2 (a) if there is no special explanation. Sampling time is set to  $5e-5$  sec. Sample significant simulation results are presented below.

Fig.4.2 shows the starting speed, current  $i_a$ , torque response and stator frame  $i_d$  versus  $i_q$  response of the proposed NFC based IM drive at no load and rated speed conditions. It is found that the NFC based IM drive has small settling time without any overshoot/undershoot and any steady state error. Moreover, the motor current is small during the steady state. The plot of stator frame  $i_d$  versus  $i_q$  shown in Fig.4.2(d), which shows the global stability of the complete drive. Starting speed and current responses of the proposed NFC based IM drive at full load ( $T_L=150N.m$ ) and different command speed conditions such as 180 (rad./sec.), 100 (rad./sec) and 30 (rad./sec.) are also shown in Figs. 4.3-4.5, respectively. The results show that the drive follows the command speed very quickly without any overshoot and nearly zero steady-state error at any command speed conditions. The current responses at different command speed conditions are sinusoidal and balanced. Thus, it is found that the performances of the proposed drive for a wide speed range are satisfactory and globally stable.

The ability to withstand disturbances is another important feature of the proposed NFC based control system. The change of load is a typical external disturbance and also for a high performance drive, the load change is a very common situation. The



speed and torque responses for the proposed drive under the operating conditions of sudden load disturbance are shown in Fig. 4.6. The motor is started without load and at  $t=1$  second the load is suddenly increased to full load  $T_L=150$  N.m. It is evident from this figure that the proposed NFC is capable of handling the load disturbance with a negligible amount of speed deviation. A comparison among the conventional PI controller, FLC and the proposed NFC is also presented in order to prove the superiority of the proposed NFC. The PI controller parameters were designed by trial and error in order to have fast speed response and minimum settling time so that it can be comparable with the proposed controller. The detailed design and structure of FLC can be found in [33]. Figures 4.7-4.8 show the speed responses for the PI (Gain\_P=20, Gain\_I=150) and FLC based IM drive under the operating conditions of sudden load disturbance, respectively. It can be found that the PI based drive system suffers a big speed drop and long recovery time, while the FLC based drive system suffers too much speed vibrations, which are not acceptable for high performance applications.

Figures 4.9-4.11 show the speed responses of the IM drive with a sinusoidal reference speed at full load ( $T_L=150$ N.m) for the proposed NFC, conventional PI (Gain\_P=500, Gain\_I=1), and conventional FLC, respectively. As shown in Figs. 4.9-4.11, the proposed NFC can follow the sinusoid speed reference without any error, whereas the PI and FLC show some speed deviations.

The comparison between the proposed NFC and the conventional FLC based IM drive for command speed reversal is also investigated. Figs. 4.12-4.13 show speed, torque, and speed error responses of the proposed NFC based IM drive for command

speed reversal at full load ( $T_L=150\text{N.m}$ ), respectively. It is shown in figure 4.12 that the drive can follow the command speed quickly without overshoot/undershoot and zero steady state error even if the command speed is changing in the opposite direction. Fig 4.14 (a)-(c) show speed, torque, and speed error responses of the conventional FLC based IM drive for command speed reversal. It can be found that the FLC based IM also suffers some speed deviations.

The ability to withstand the motor parameter variations is another important criterion of the control system, particularly for the IM drive where the motor parameters are affected by saturation and temperature effects. The speed and the corresponding actual phase current responses are shown in Figs 4.15 (a) and (b), respectively, where mutual inductance  $L_m$  is increased by two-fold, under full load ( $T_L=150\text{N.m}$ ) and rated speed conditions. It is shown that the drive can follow the command speed even after a change of mutual inductance. Figs 4.16(a) and (b) show the speed and the corresponding phase current responses of the NFC based IM drive, respectively with doubled rotor inertia and full load ( $T_L=150\text{N.m}$ ) conditions. The results show that the drive follows the rated command speed smoothly even with doubled rotor inertia. Because of increased inertia the time to reach the steady state is slightly greater. The speed and the corresponding actual phase current responses are shown in Figs. 4.17(a) and (b), respectively, where rotor resistance  $R_r$  is increased twofold, under full load and rated speed conditions. It can be found that the drive follows the command speed with only some negligible dent. Hereby, it is shown that the proposed NFC based IM drive is capable of handling the variation of parameters.

In order to prove that the proposed NFC doesn't need precise IM drive model, Fig. 4.18 shows the starting speed response, current response and torque response of a 3 hp IM drive model based on the proposed NFC. Only learning rate  $\eta$  and torque limitation of the proposed NFC have been readjusted for the new motor and found that the performance of the proposed NFC based 3 hp IM is almost similar to the previously considered 50 hp motor. Thus, the proposed NFC is found to be easy-build for various size of motor drive.

Fig. 4.19 shows the starting speed and current response of the proposed NFC based IM in the case of only two membership functions for each input. Though a tiny oscillation occurs in the speed response at beginning of steady state, the proposed NFC based IM drive still exhibits small settling time without any overshoot and steady state error. Therefore, the three membership function based NFC is recommended. The proposed NFC based IM drive has been found robust for high performance industrial drive applications.

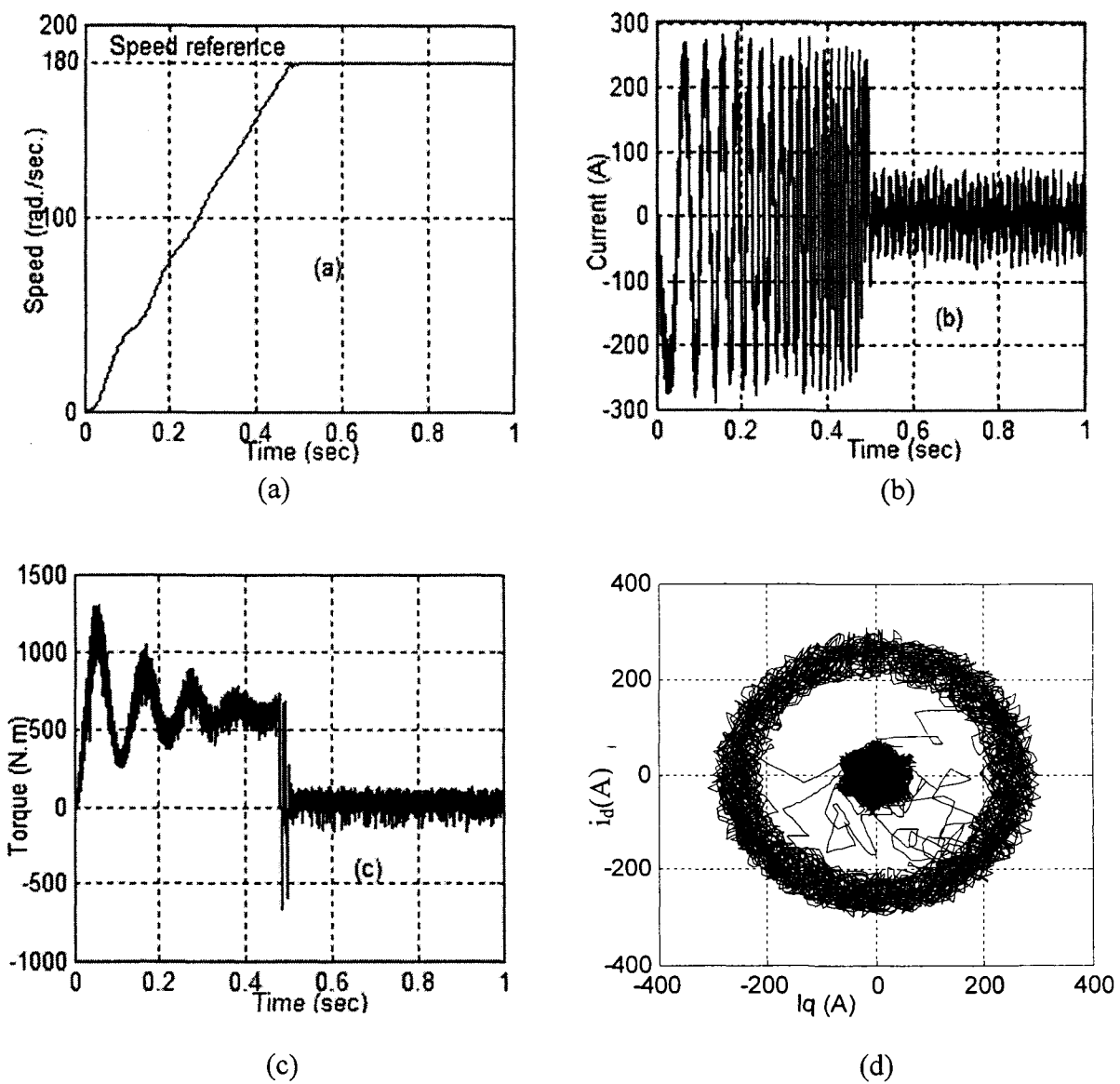
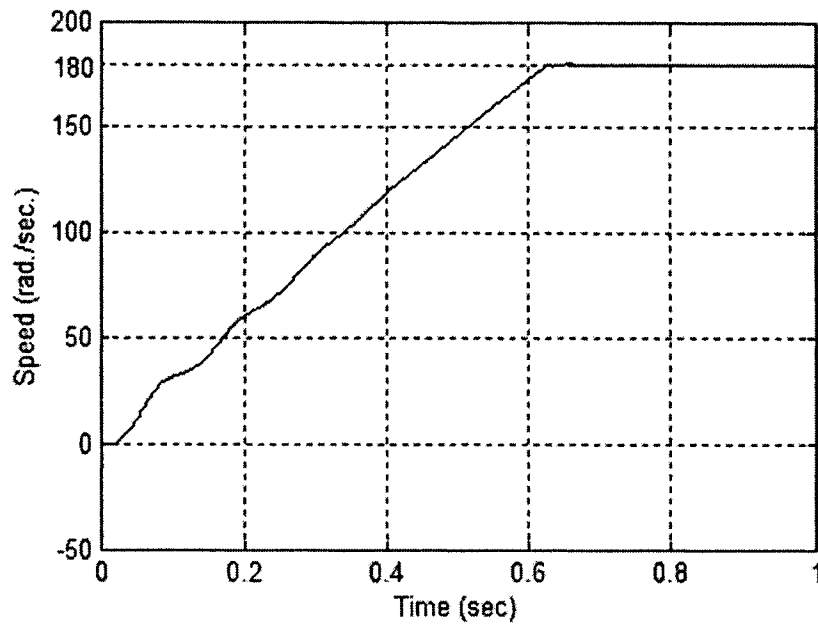
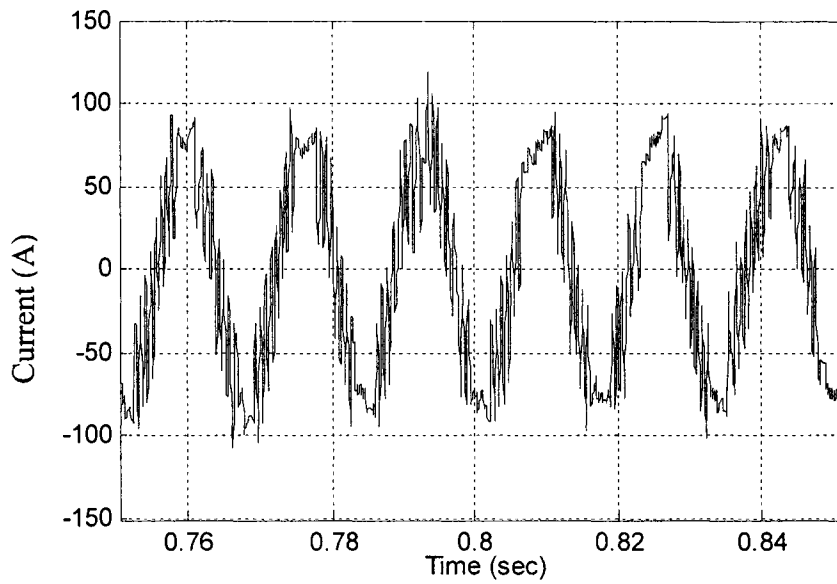


Fig 4.2: Simulated starting responses of the drive with the proposed NFC: (a) speed, (b) current  $i_a$ , (c) torque and (d) stator frame  $i_d$  versus  $i_q$  response.

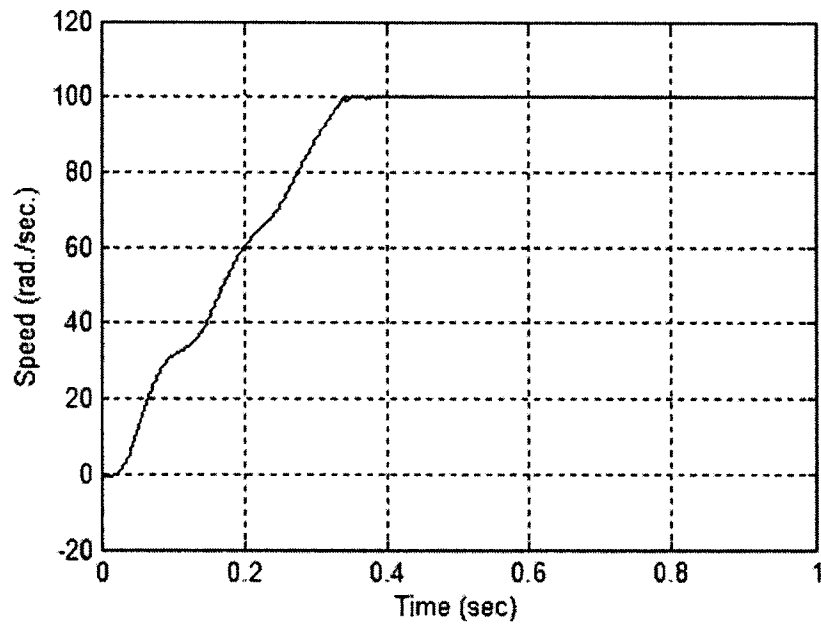


(a)

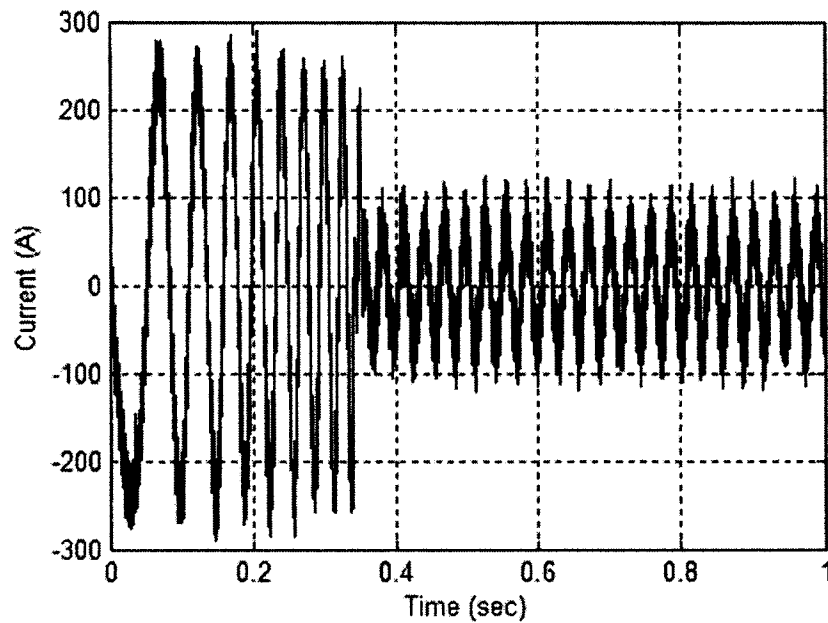


(b)

Fig 4.3: Simulated starting responses of the drive with NFC at full load (150 N.m) and rated speed (180 rad./sec.) conditions: (a) speed, and (b) steady-state actual a-phase current.

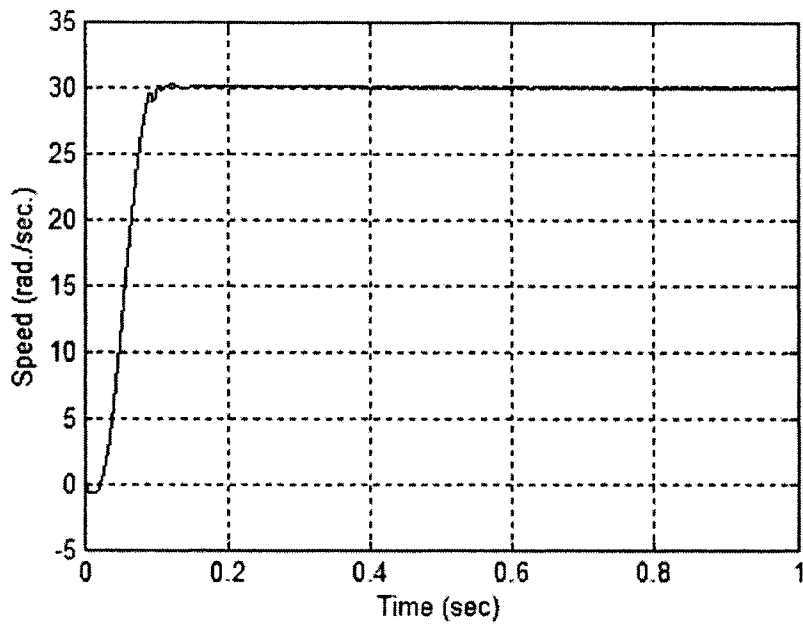


(a)

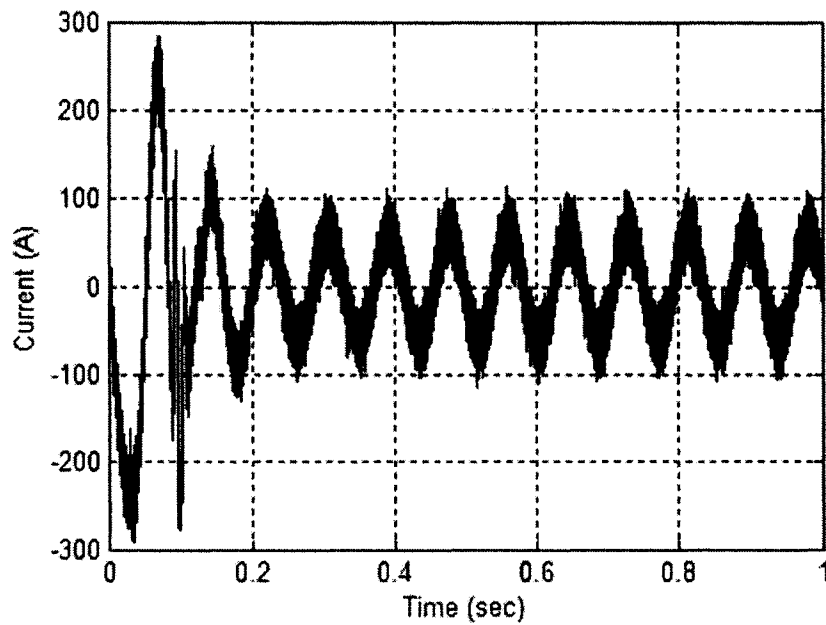


(b)

Fig 4.4: Simulated starting responses of the drive with NFC at full load (150 N.m) and  $\omega_r^* = 100$  rad./sec.: (a) speed, and (b) current  $i_a$ .

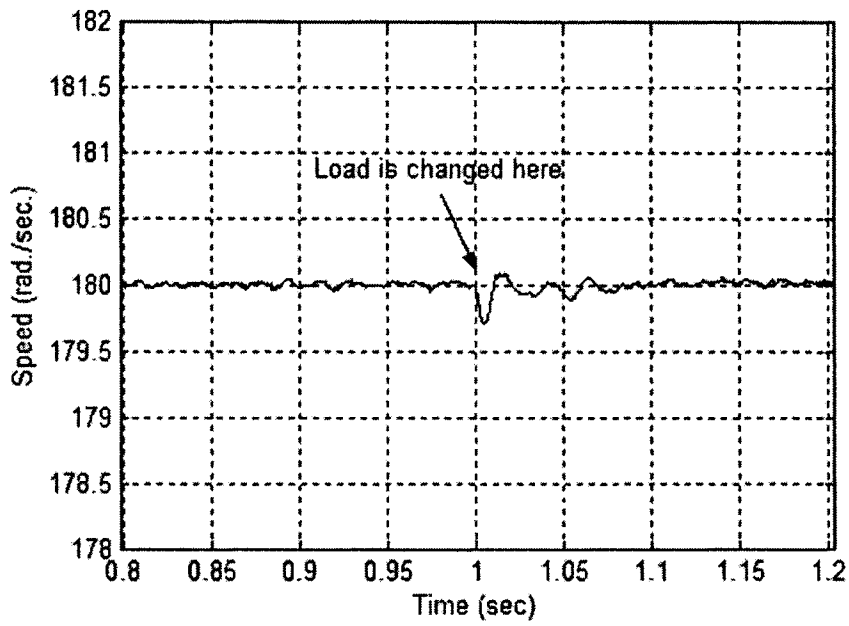


(a)

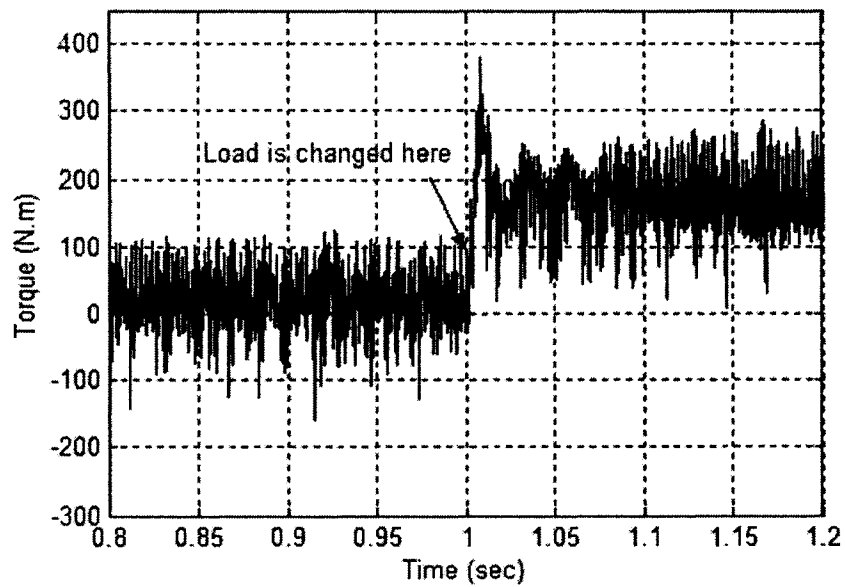


(b)

Fig 4.5: Simulated starting responses of the drive with NFC at full load (150 N.m) and low command speed (30 rad./sec.) conditions: (a) speed, and (b) current  $i_a$ .



(a)



(b)

Fig.4.6: Simulated responses of the drive with NFC for a step increase in load ( 0N.m → 150N.m): (a) speed, and (b) torque.



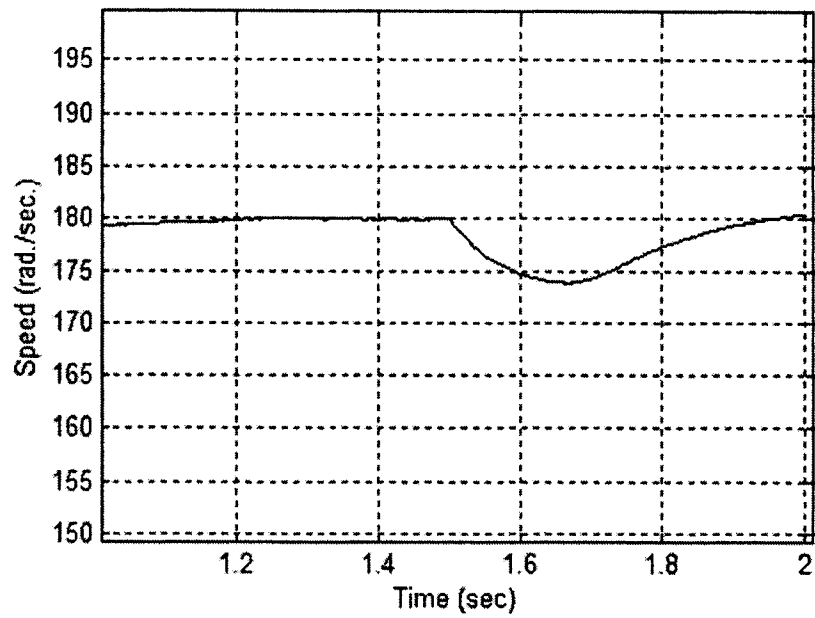


Fig.4.7: Simulated speed responses of the drive with PI controller for a step increase in load (0N.m  $\rightarrow$  150N.m).

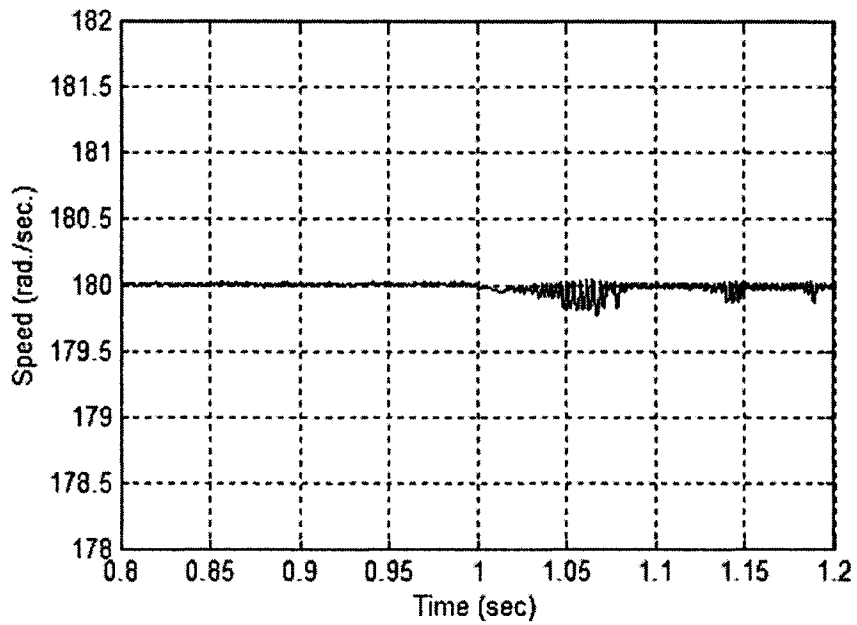


Fig.4.8: Simulated speed responses of the drive with FLC for a step increase in load (0N.m  $\rightarrow$  150N.m).

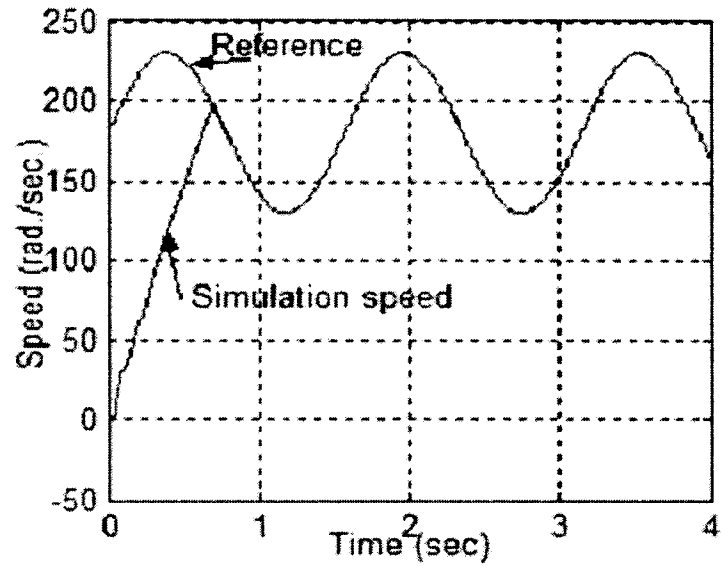


Fig.4.9: Simulated speed response of the drive at full load with NFC for a sinusoidal speed reference.

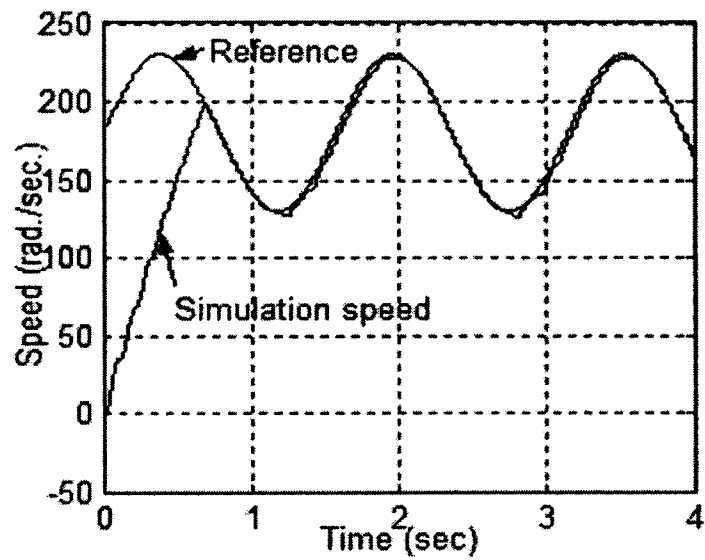


Fig 4.10: Simulated speed response of the drive at full load with PI controller for a sinusoidal speed reference.

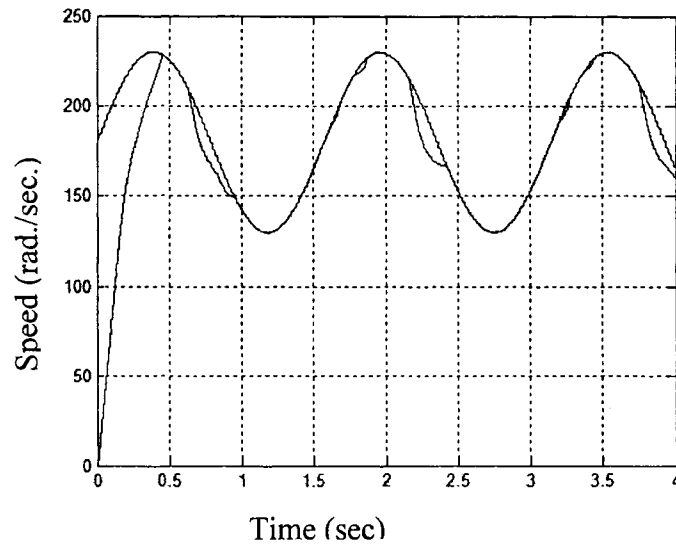


Fig 4.11: Simulated speed response of the drive at full load with FLC for a sinusoidal speed reference.

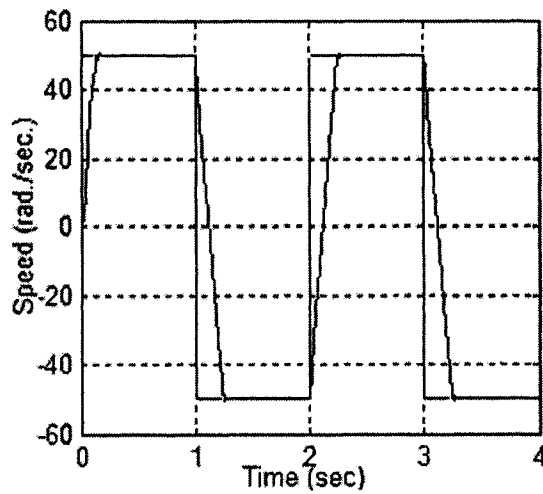
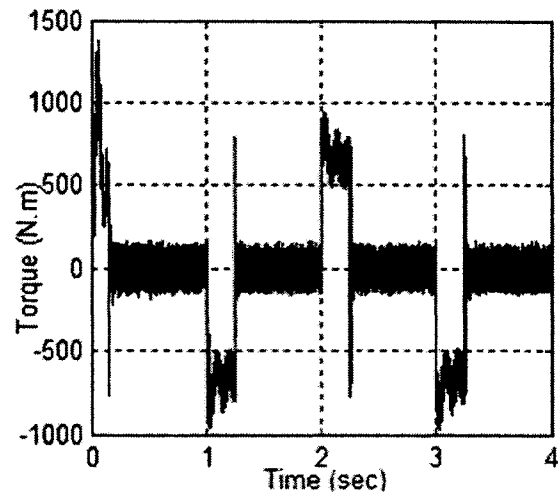
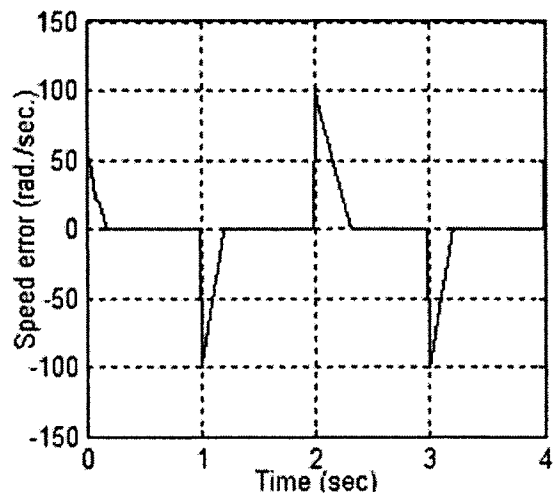


Fig 4.12: Speed response of the proposed drive at full load for speed reversal.



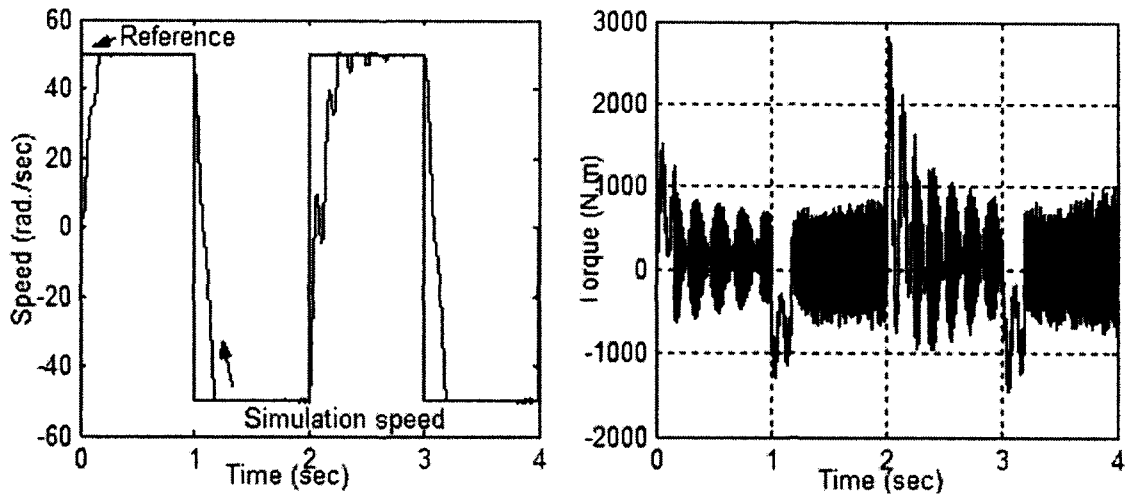
(a)



(b)

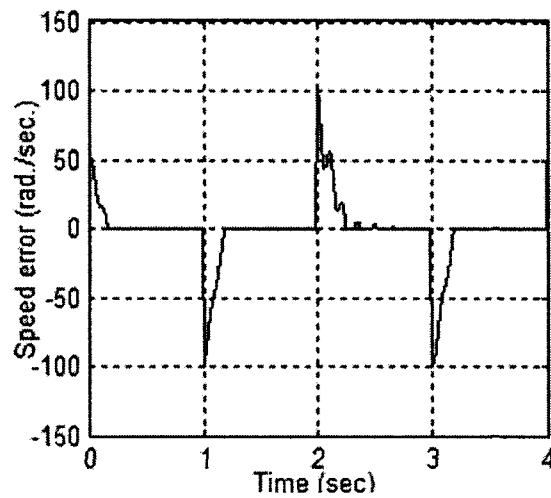
Fig.4.13: Simulated responses of the NFC based drive at full load for speed reversal:

(a) torque, and (b)  $\Delta\omega$ .



(a)

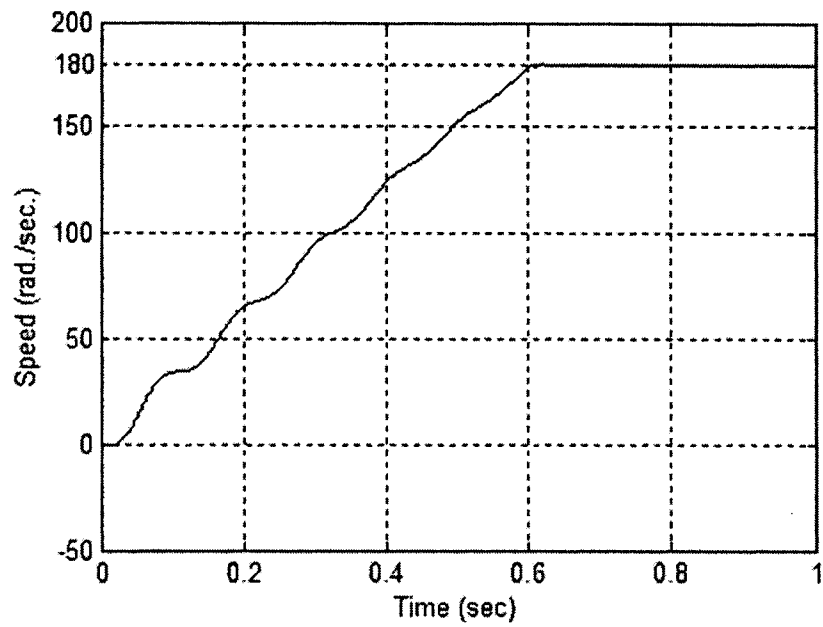
(b)



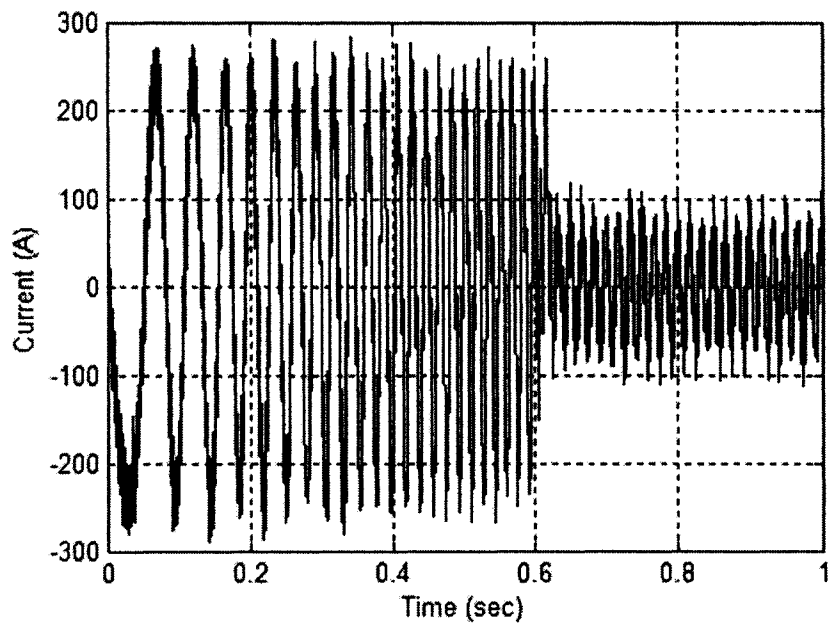
(c)

Fig.4.14: Simulated responses of the FLC based drive at full load for speed reversal:

(a) speed, (b) torque, and (c)  $\Delta\omega_r$ .

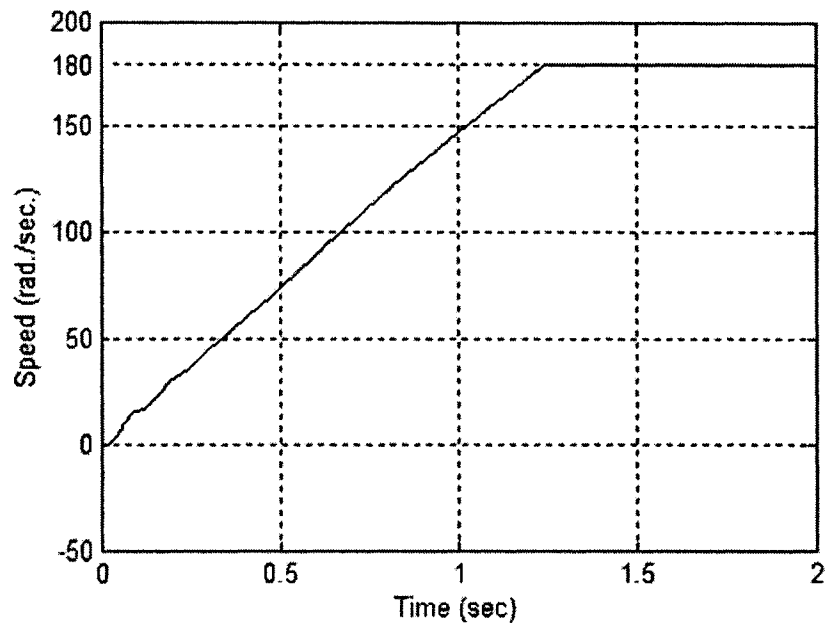


(a)

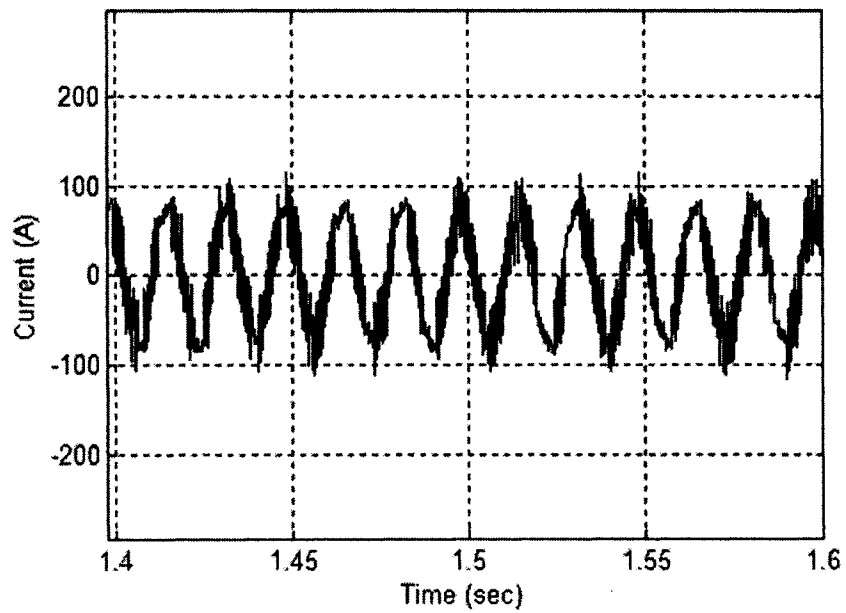


(b)

Fig.4.15: Simulated speed response of the proposed NFC based drive at rated load for doubled magnetizing inductance: (a) speed, and (b) current  $i_a$ .

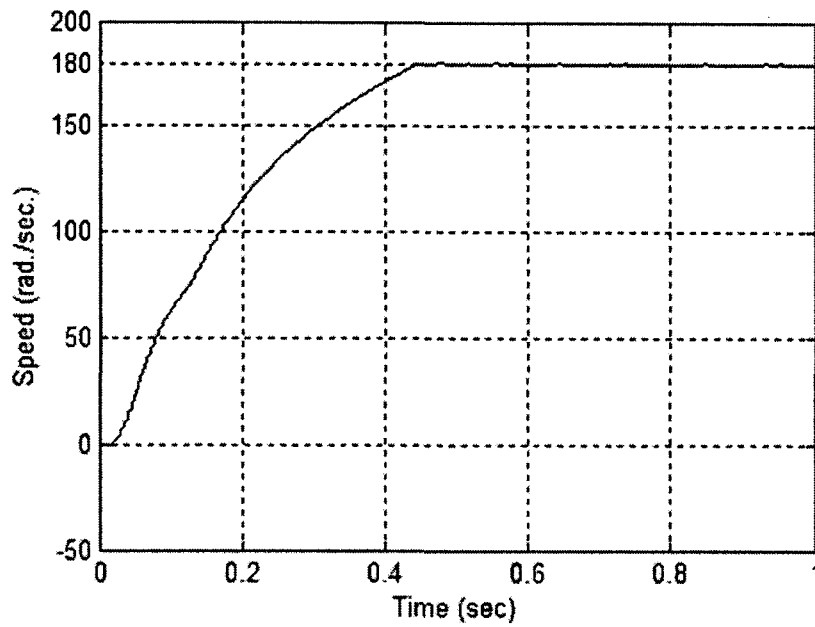


(a)

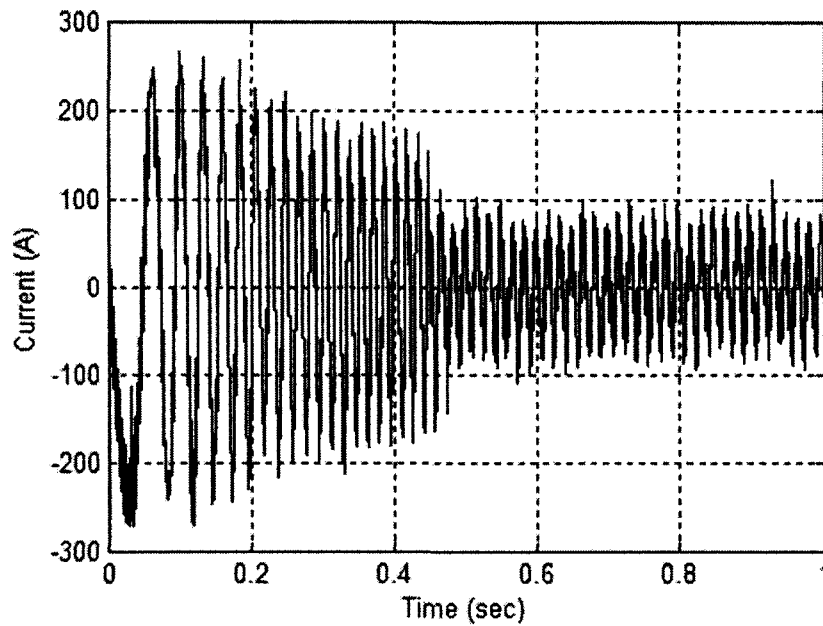


(b)

Fig.4.16: Simulated speed response of the proposed NFC based drive at rated load for doubled  $J_m$ : (a) speed, and (b) current  $i_a$ .



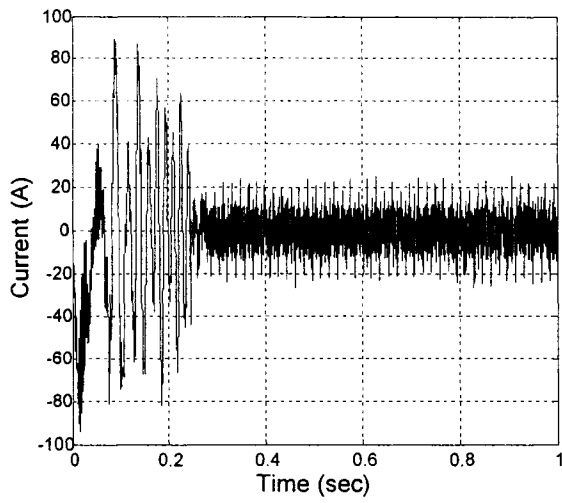
(a)



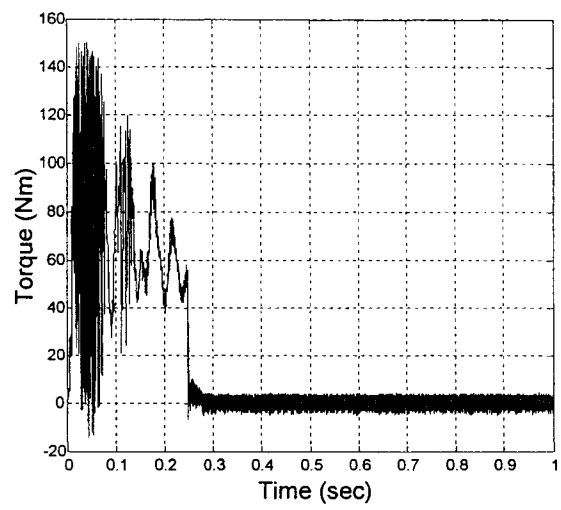
(b)

Fig.4.17: Simulated speed response of the proposed NFC based drive at rated load for doubled rotor resistance: (a) speed, and (b) current  $i_a$ .

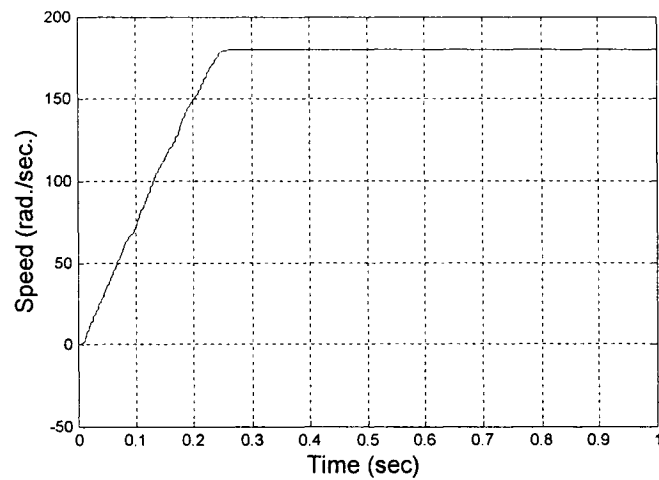




(a)

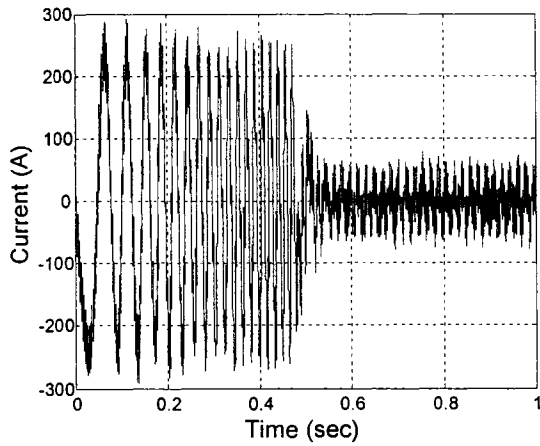


(b)

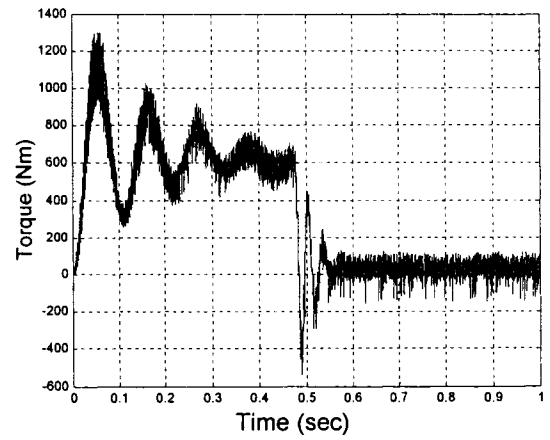


(c)

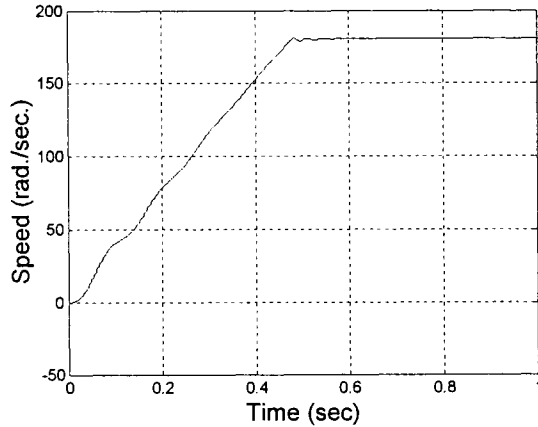
Fig.4.18: Simulated starting responses of the proposed NFC based 3HP IM drive without load: (a) current  $I_a$ , (b) torque, and (c) speed.



(a)



(b)



(c)

Fig.4.19: Simulated starting responses of the drive with 2 membership functions NFC without load: (a) current  $I_a$ , (b) torque, and (c) speed.

## 4.3 Summary

A complete FOC-IM drive incorporating the proposed NFC has been presented in this chapter. The simulation results show encouraging performances of the proposed drive. The NFC can adjust itself with different operating conditions such as load change, parameter variations and step change of command speed. Therefore, the NFC can be a good substitute for the conventional fixed gain PI or conventional fuzzy-logic controllers. However, in this chapter the motor was controlled only up to the rated speed since the rotor flux was assumed constant. If the speed increases above rated speed, then the voltage and current ratings of motor and inverter exceeds the rated limit. In order to control the motor above the rated speed within the safe operating area, the flux must be weakened. Moreover, if the flux is not estimated properly below the rated speed, there will be torque pulsations and hence vibrations, which are not acceptable for high performance drives. Therefore, a rotor flux estimation method is developed which will be discussed in the next chapter.

## Chapter 5

# Design of Model Reference Adaptive Rotor Flux Observer

As mentioned in the summary of chapter 4, in order to control the motor at high-speed conditions (above the rated speed), good rotor flux estimation for flux weakening is required. Particularly, the rotor flux, which cannot be measured directly, needs to be estimated properly. Otherwise, the motor and converter voltages and current will exceed the rated limits. Furthermore, there will be torque pulsations and hence speed vibrations which is not acceptable for high performance drives. The rotor flux can be estimated based upon open loop voltage model and current model [56-57]. Their advantages and disadvantages are well known. In order to combine the advantages of both models a closed loop Gopinath flux observer model has also been reported [58]. However, the existing flux observer methods just estimate the rotor flux based on voltage, current and speed, but they do not force the motor to follow the reference flux trajectory. In this thesis, a model reference adaptive flux (MRAF) [59]

observer is presented based on a reference flux model and a closed loop Gopinath model [54], which combines current and voltage model flux observers.

## 5.1 Closed Loop Flux Observer Model

Sensors of flux and speed or position of the rotor spoil the ruggedness of IM drive systems. Therefore, there is tendency to replace them with observers which convert the stator voltage and current signals into the required information concerning other variables of the motor. Flux observers used in vector control systems are either of an open-loop or closed-loop type. Basically, there are two types of open-loop flux observers which are current model and voltage model. Equation (2.10) can be rewritten as [4],

$$\lambda_s^s = \frac{L_m}{L_r} \lambda_r^s + \sigma L_s i_s^s \quad (5.1)$$

and

$$i_r^s = \frac{1}{L_r} (\lambda_r^s - L_m i_s^s) \quad (5.2)$$

where  $\sigma$  denotes the so-called total leakage factor, defined as  $\sigma = 1 - \frac{L_m^2}{L_s L_r}$ .

Substituting equations (5.1) and (5.2) in equations (2.8) and (2.9), the expression of voltage and current model flux observer can be obtained as

$$p \lambda_r^s = \frac{L_r}{L_m} (v_s^s - (R_s + \sigma L_s p) i_s^s) \quad (5.3)$$

and

$$p\lambda_r^s = (j\omega_r - \frac{1}{\tau_r})\lambda_r^s + \frac{L_m}{\tau_r}i_s^s \quad (5.4)$$

The well-known closed loop Gopinath flux observer model is based on open loop voltage model and current model flux observers as shown in Fig.5.1. As the voltage model flux observer works better for high speeds and current model flux observers works better for low speeds, the combined closed loop flux observer model works for both nominal and low speeds.

## 5.2 MRAF Rotor Flux Regulation

In order to achieve high speeds, the stator current frequency is increased. The stator voltage is directly proportional to the motor flux and the angular speed. In

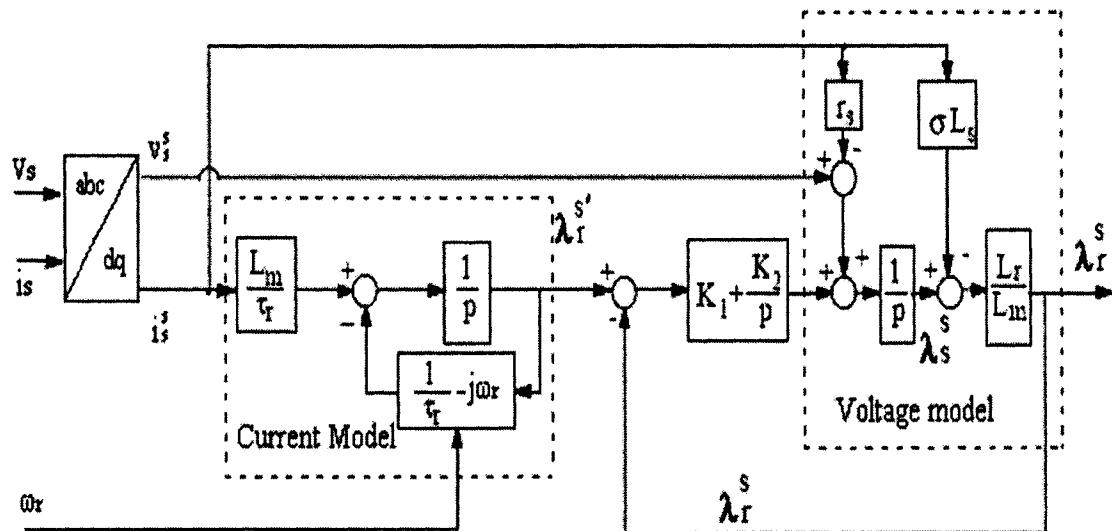


Fig.5.1: Closed loop Gopinath flux observer.

normal condition the motor flux is kept constant. A maximum stator speed is reached with the limit output voltage of the power converter. To reach a higher speed the flux is reduced as an invert of the angular speed in order to keep the stator voltage constant and equal to its maximum. The reference flux model is built with this well-known constant flux and flux weakening methods, which are given by,

$$\lambda_{ref} = \lambda_{rat} , \text{ when } \omega_r < \omega_{rat} \quad (5.5)$$

$$\lambda_{ref} = \lambda_{rat} * \omega_{rat} / \omega_r , \text{ when } \omega_r > \omega_{rat} \quad (5.6)$$

The block diagram of the proposed MRAF observer is shown in Fig.5.2. It is mainly composed of reference flux model, closed loop Gopinath rotor flux observer model and a PI compensator for the reference model. This model is proposed in this thesis in order to follow a reference rotor flux trajectory  $\tilde{\lambda}$  instead of just estimating the flux  $\hat{\lambda}$  based on voltage, current and speed. Thus the command d-axis rotor flux linkage is calculated  $\lambda_d^*$  from the proposed MRAF observer.

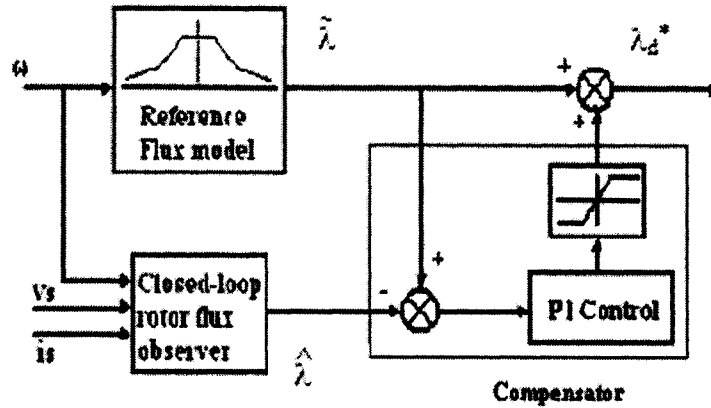


Fig.5.2: Proposed MRAF observer

### 5.3 Simulation of the MRAF Observer Based NFC for IM Drive.

In order to investigate the performance of the proposed MRAF based NFC, numerous simulation tests were performed under different operating conditions in Matlab/Simulink [53]. Sample simulation results are shown here.

Figure. 5.3 shows the starting speed, torque, rotor flux and stator current responses of the IM drive with the proposed MRAF based NFC. The motor was started with 150 N.m load and a step speed command of 150 rad./sec. It is found from Fig. 5.3(a) that the NFC based IM drive has a small settling time without any overshoot/undershoot and any steady state error. The estimated flux linkage of the closed loop flux observer is tracking the reference rotor flux as shown in Fig. 5.3(b).

In order to investigate the performances of the drive in flux weakening region, speed, torque and flux responses for a high command speed of 300 rad./sec with a



nonlinear load ( $T_L=0.1*\omega_r+0.01*\omega_r^2+5$  N.m) and a constant load (100 N.m) are shown in Fig. 5.4 and 5.5, respectively. It is found from both Fig. 5.4(a) and Fig. 5.5(a) that the NFC based IM drive can follow a high-speed trajectory without any overshoot/undershoot and any steady state error. Also, the estimated flux linkage can follow the flux-weakening trajectory very well as shown in Fig 5.4(c) and Fig 5.5(c). The performance of the proposed IM drive incorporating the MRAF observer based NFC is found satisfactory in terms of speed tracking and flux estimation.

## 5.4 Experimental Setup

In order to implement the control scheme in real time the DSP board DS1104 is used. The board is installed in an Intel PC with uninterrupted communications through dual port memory. The DS1104 board is mainly based on a 64-bit floating-point MPC8240 processor with PPC603e core. The DSP is supplemented by a set of on-board peripherals used in digital control systems including analog to digital (A/D), digital to analog (D/A) converters, digital I/O, serial interface and incremental encoder interfaces. Also, it is equipped with a TI 16-bit micro controller TMS320F240 DSP that acts as a slave processor and provides the necessary digital I/O ports and powerful timer functions such as input capture and PWM generations. The block diagram of the hardware schematic is shown in Fig. 5.6. The actual motor currents are measured by the Hall-effect sensors and then fed back to the DSP board through the A/D channel. Rotor position is sensed by an optical incremental encoder.

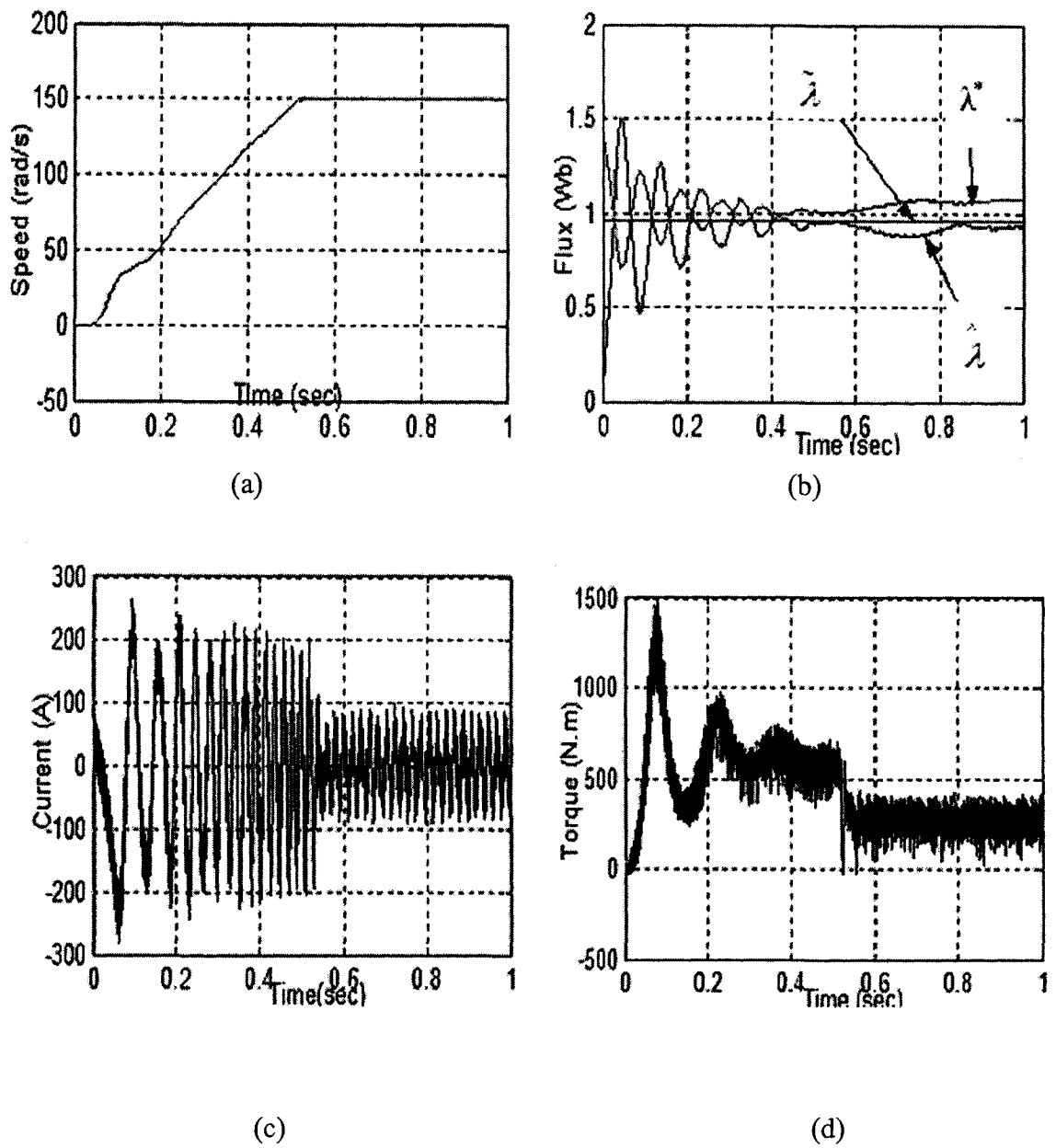
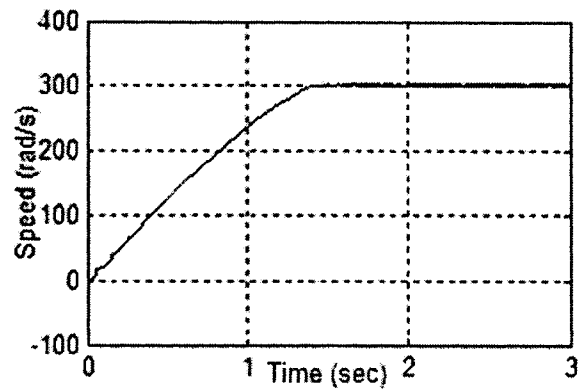
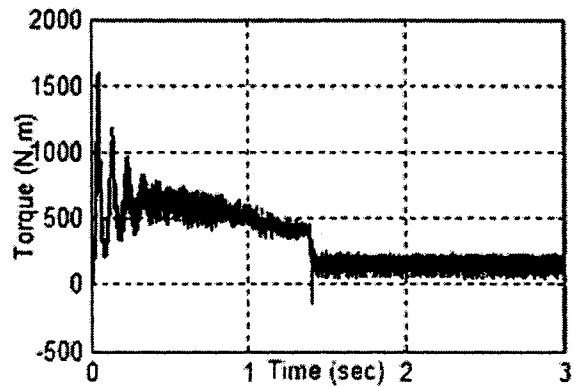


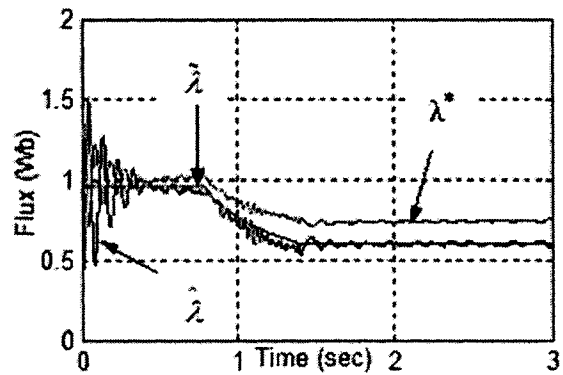
Fig.5.3: Simulated starting responses of the proposed MRAF based NFC for IM drive with  $T_L=150$  N.m; (a) speed, (b) flux, (c) current  $i_a$ , and (d) torque.



(a)

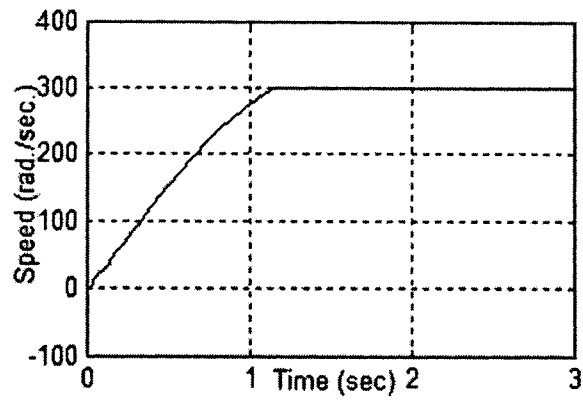


(b)

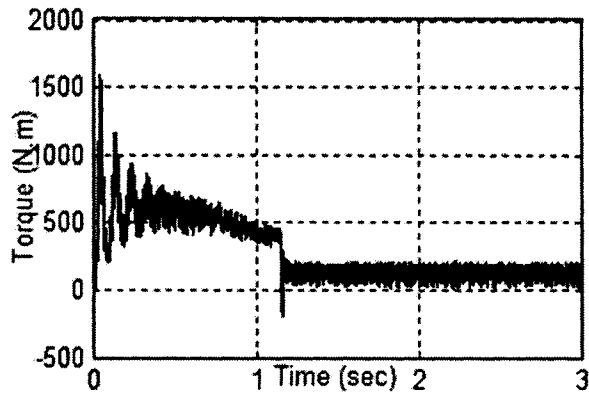


(c)

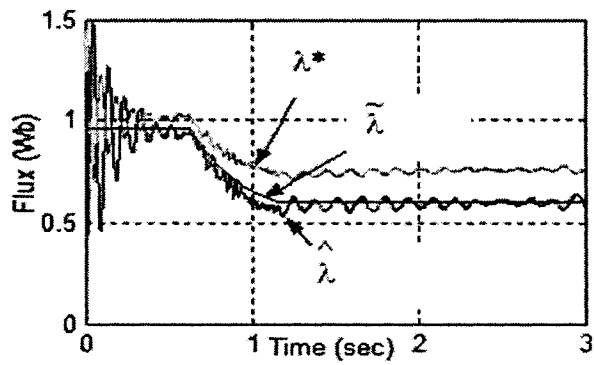
Fig.5.4: Simulated responses of the drive of MRAF based NFC for a high speed command of 300rad/s with a nonlinear load; (a) speed, (b) torque, and (c) flux.



(a)



(b)



(c)

Fig.5.5: Simulated responses of the drive of MRAF based NFC for a high speed command of 300rad/s with load=100 N.m; (a) speed, (b) torque, and (c) flux.

mounted at the rotor shaft and is fed back to the DSP board through the encoder interface. The outputs of the DSP board are six PWM signals that are sent directly to the base drive circuit of the inverter.

The control algorithm is implemented in real time by using Matlab Simulink and real-time toolbox. A real-time Simulink model is developed for the complete drive which is shown in Appendix B.7. The program is downloaded to the DSP Control-desk. As the position encoder and other encoder circuits are not fully integrated, the experimental results are not obtained due to time constraint.

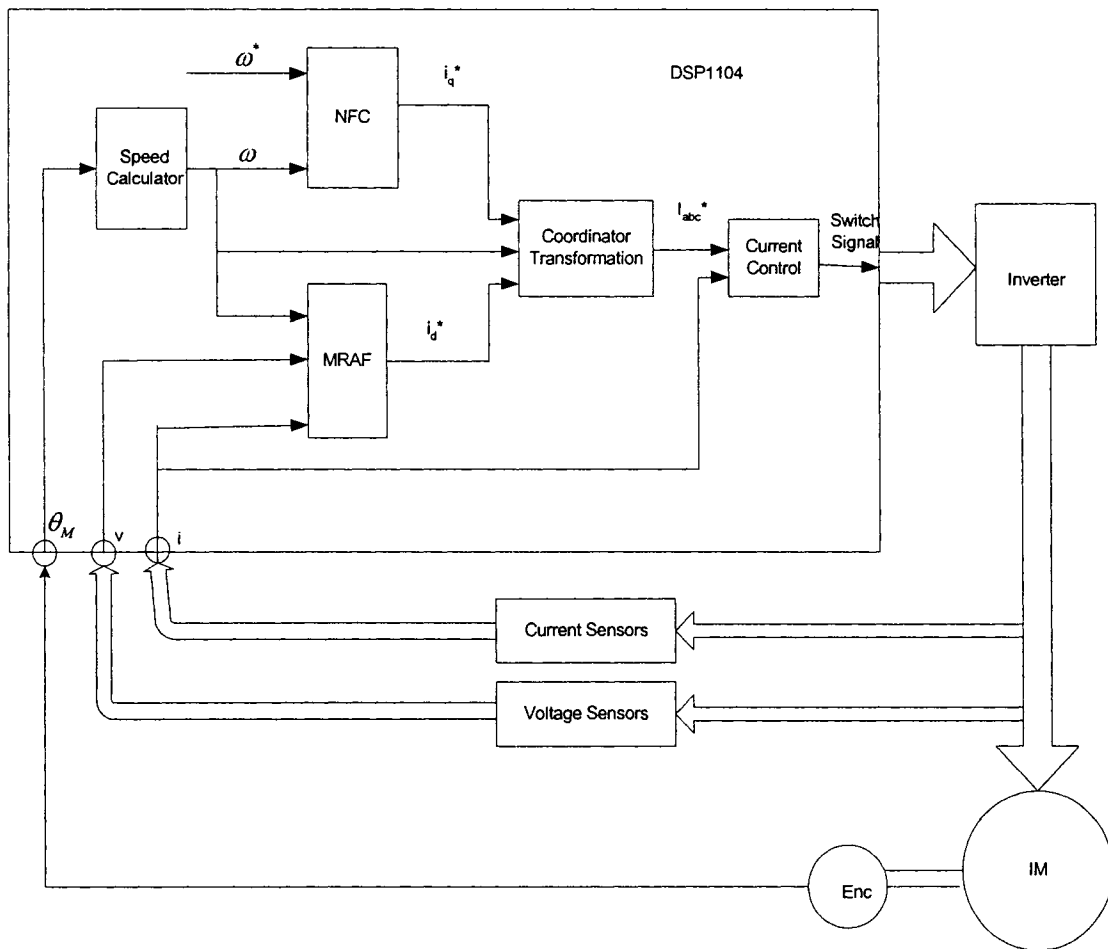


Fig.5.6: Block diagram of the hardware schematic of the VSI-fed IM drive.

# Chapter 6

## Conclusion

In chapter 1 the review of IM with various control techniques has been provided. This identifies the problems of controlling the electric motors in high performance variable speed drive applications. Problems of controlling the speed accurately for an IM with different dynamic operating conditions have been identified and the NFC has been proposed to overcome these problems.

In chapter 2 the mathematical model of the IM was derived in the excitation reference frame. Coordinates transformation was used to convert the conventional a-b-c parameters to the d-q axes frame. It was clear that the q-axis current controlled the torque, and the d-axis current controlled the flux. Thus, the FOC based IM drive mathematical model is formed and presented. The working principles of a VSI and a hysteretic current controller are also presented in order to make sure that the actual motor phase currents  $i_a$ ,  $i_b$  and  $i_c$  can follow the corresponding command currents  $i_a^*$ ,  $i_b^*$  and  $i_c^*$ .

Chapter 3 briefly described the fundamentals of the fuzzy logic controller and neural network. The basic ideas of fuzzy logic, fuzzy sets, membership functions, fuzzy inference engine and defuzzification have been presented. The development of a neuro-fuzzy logic speed controller incorporating FLC to ANN has been presented in details.

In chapter 4, a complete FOC-IM drive using the proposed NFC has been developed. The performance of the proposed NFC has been investigated through extensive simulations. The starting performances at various speed, sudden speed changes and parameter variations of the proposed drive have been investigated in this chapter. The NFC can adjust itself with different operating conditions such as load change, parameter variations and step change of command speed. Thus, the simulations results show encouraging performance of the proposed drive.

In chapter 5, a MRAF for the proposed NFC based IM drive is presented, so that the drive system can follow command speed trajectory over rated speed. Sampling simulation results of the proposed drive system are also shown in this chapter.

## 6.1 Achievements of the Thesis

Throughout the work the accomplishments are listed below:

- A neuro-fuzzy speed controller for FOC-IM drive has been developed.
- A complete NFC based IM drive has been built in Matlab/Simulink.

- Performances of the proposed NFC based IM drive have been extensively investigated in simulations. Comparisons between the proposed NFC and FLC, as well as the PI controller have been provided.
- The MRAF observer for the NFC based IM drive has been developed.
- Performances of the proposed MRAF observer for the NFC based IM have been investigated.
- Real-time Simulink model for the complete drive has also been developed.

## 6.2 Future Scope of the Work

As can be seen in Chapter 5, the real time implementation of the complete drive system has not been completed yet due to time constraints. As a future scope, the first step should be the real-time implementation, which has been carrying on. Also, a speed sensorless approach can be integrated with the proposed control scheme. This will eliminate the position encoder. It can be found in Chapter 3, that the learning rate  $\eta$  of the proposed NFC is decided by trial and error. To find out a self-tuning method for learning rate  $\eta$  is another challenge for future works.



# Appendix A

## IM Parameters

1)

Number of phases = 3

Number of poles = 4

Rated Frequency = 60 Hz

Rated power = 50 HP

Rated input line-to-line voltage = 460 V

Stator resistance = 0.087  $\Omega$ ,

Stator self inductance = 0.8 mH

Rotor resistance = 0.228  $\Omega$

Rotor self inductance = 0.8 mH

Mutual inductance = 34.7 mH

Rotor inertia = 1.662 kg.m<sup>2</sup>

2)

Number of phases = 3

Number of poles = 4

Rated Frequency = 60 Hz

Rated power = 3 HP

Rated input line-to-line voltage = 220 V

Stator resistance =  $0.435 \Omega$ ,

Stator self inductance = 2 mH

Rotor resistance =  $0.816 \Omega$

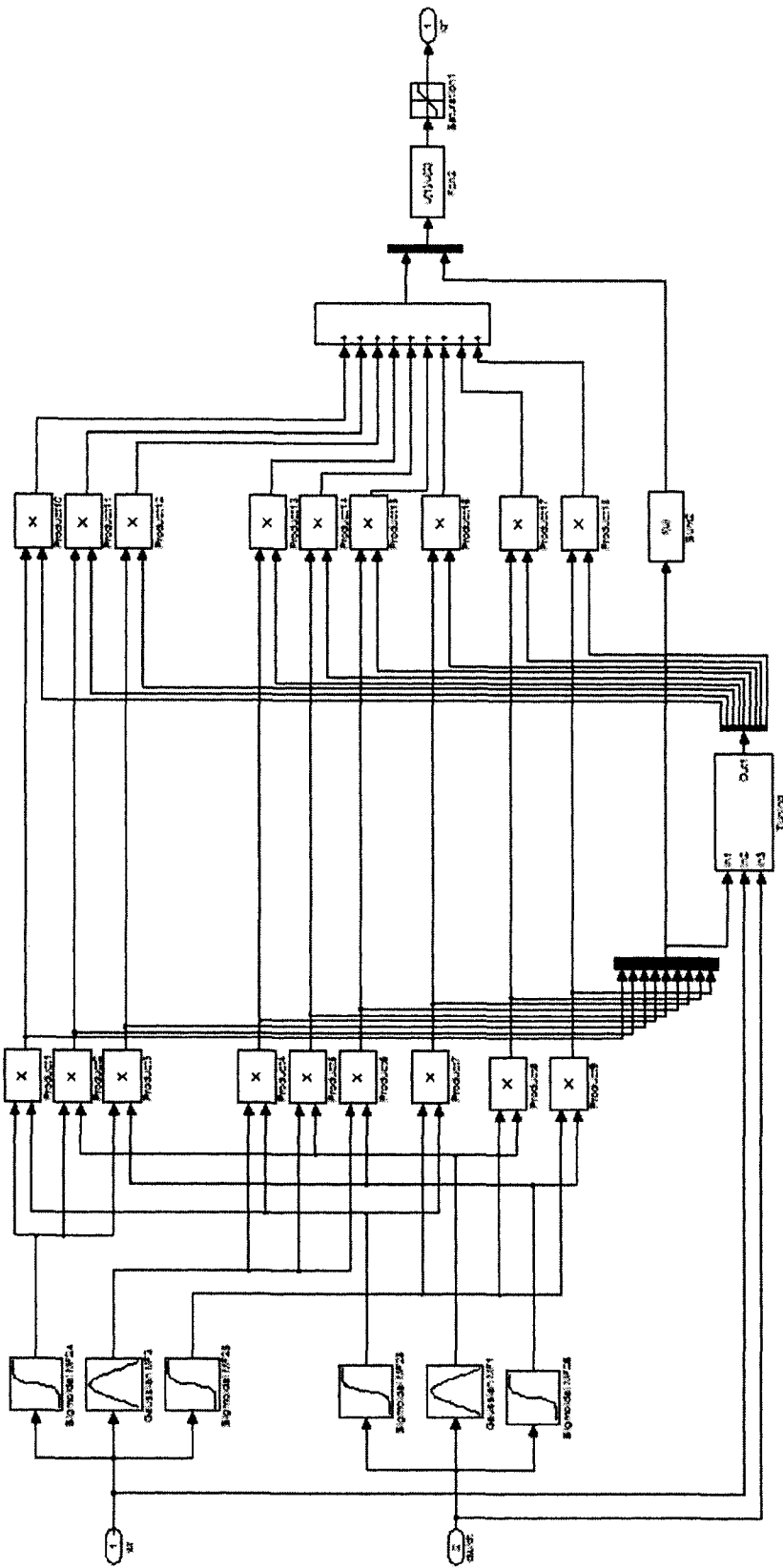
Rotor self inductance = 2 mH

Mutual inductance = 70 mH

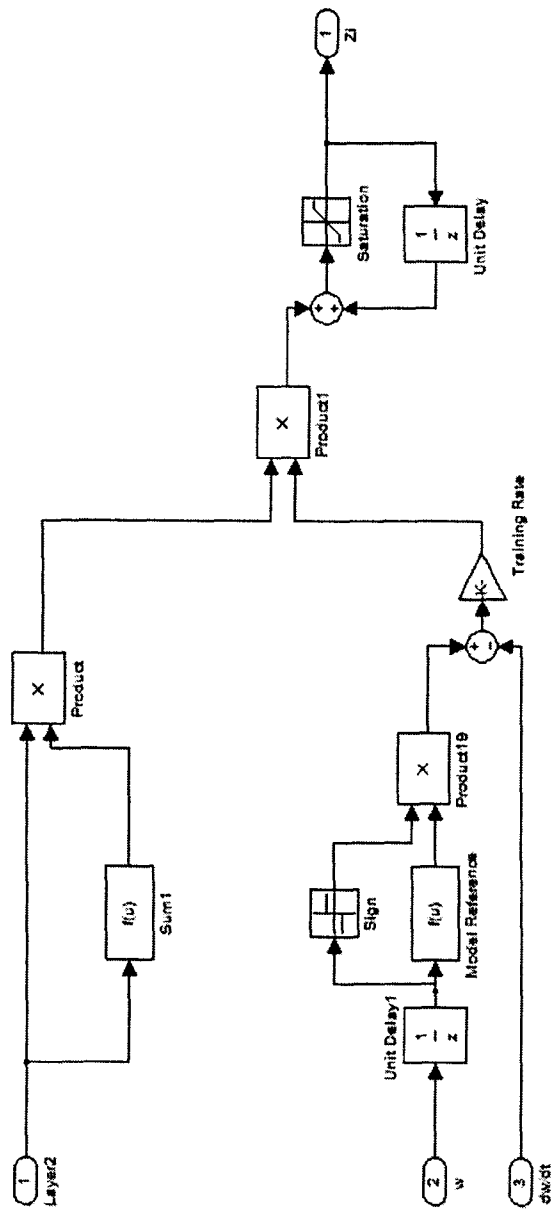
Rotor inertia =  $0.089 \text{ kg.m}^2$

# Appendix B

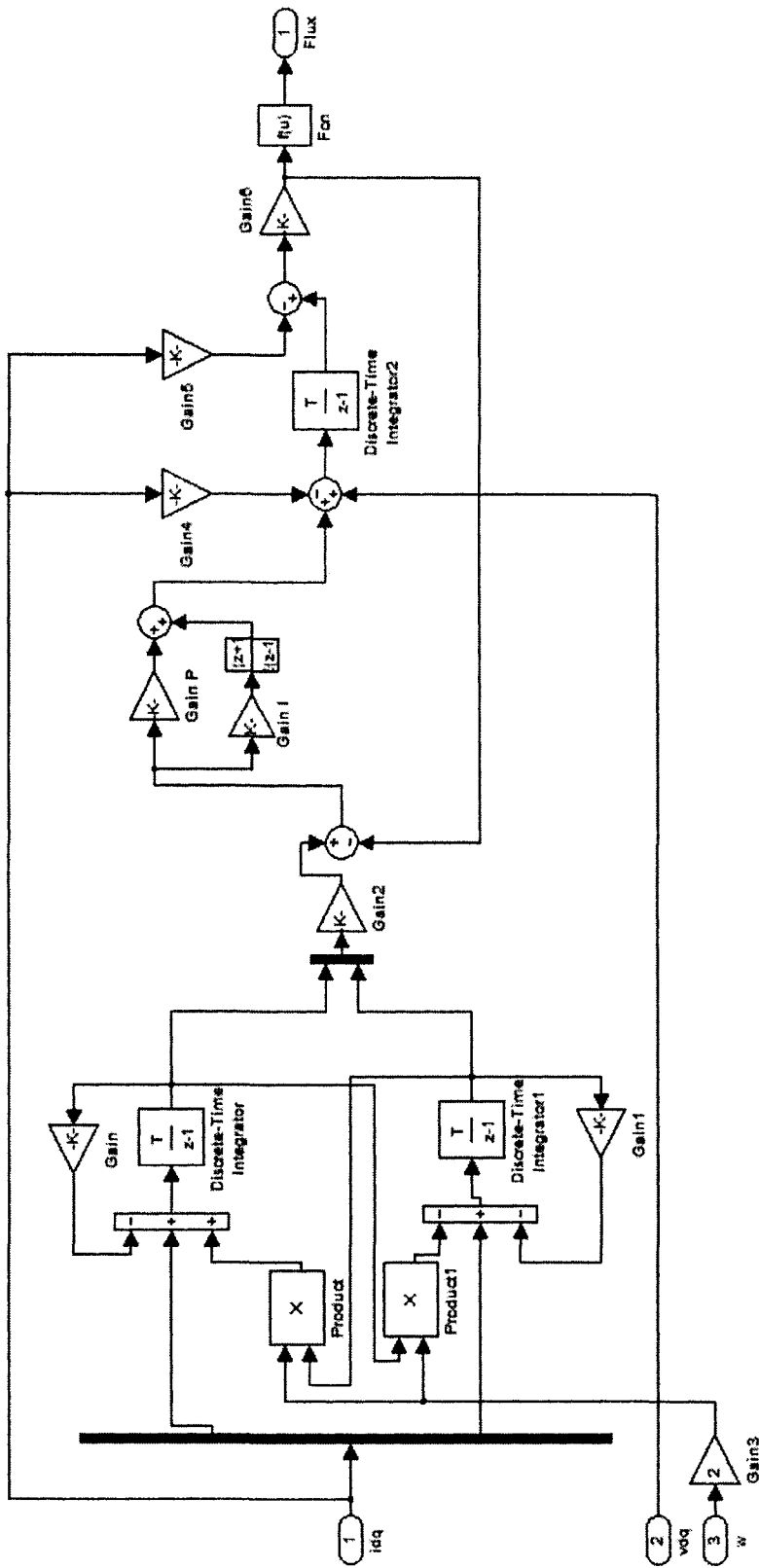
## Simulink Simulation



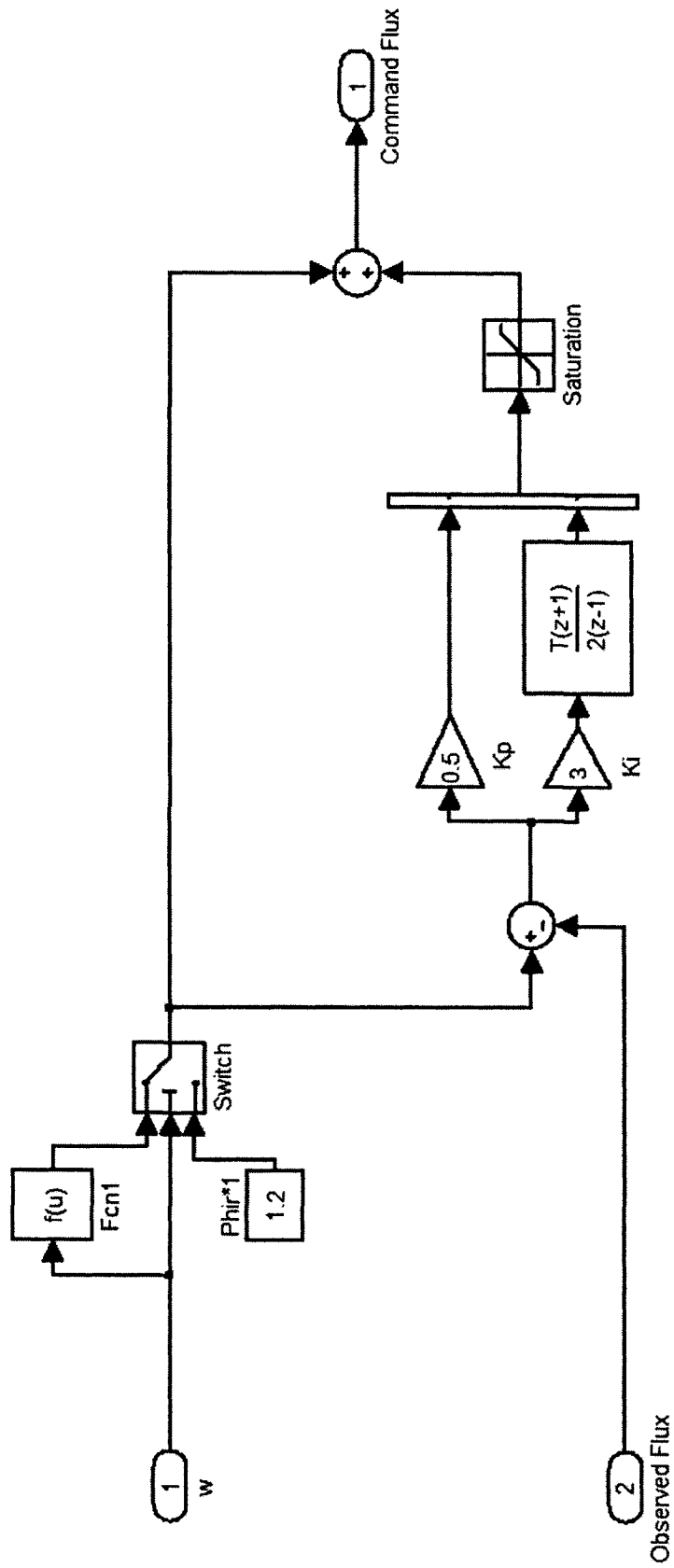
B.1 Proposed NFC Subsystem



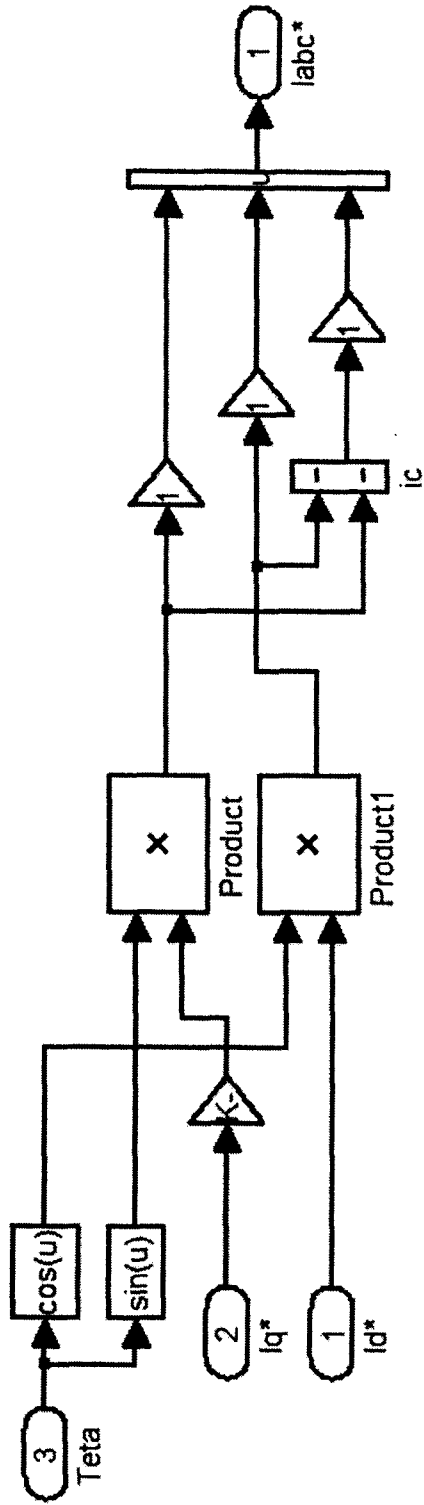
B.2 NFC Training Subsystem



B.3 Flux Observer Subsystem

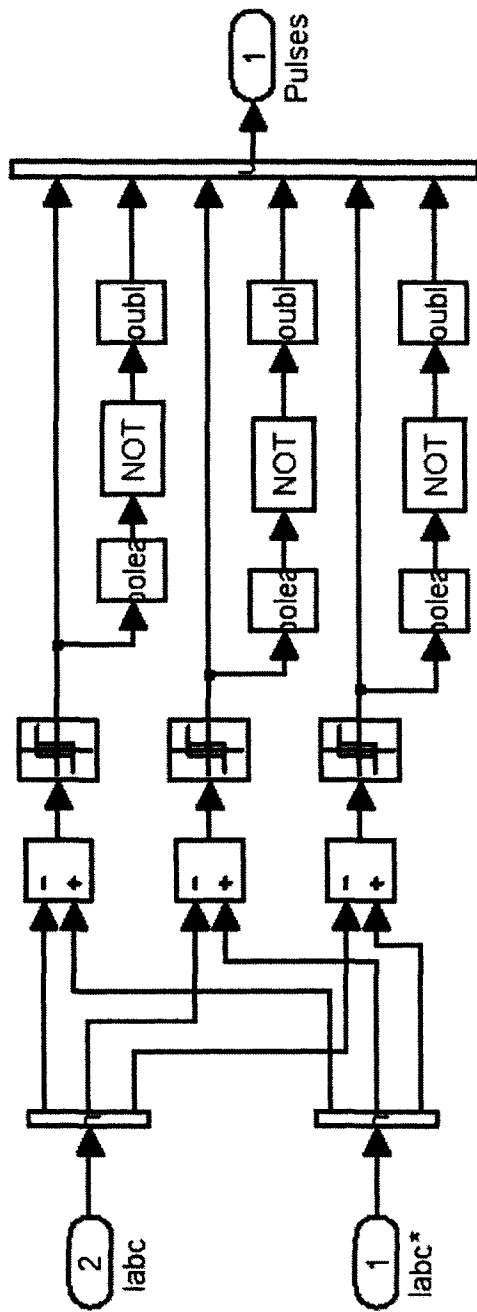


B.4 MRAF Subsystem

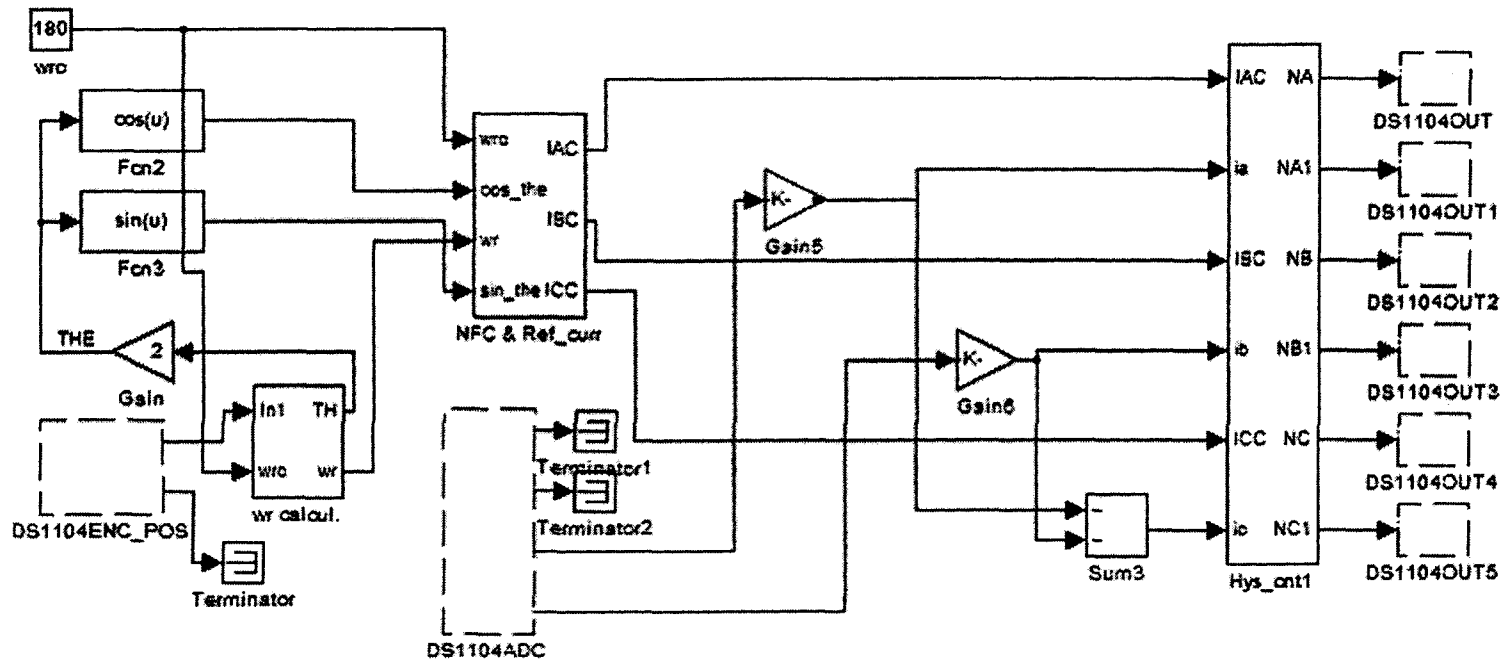


B.5 Coordinate Transformation Subsystem





B.6 Hysteretic Current Controller Subsystem



B.7 Real-Time Simulink Model for the NFC based IM drive.

# Bibliography

- [1] Cochran, Paul L., *Polyphase Induction Motors: Analysis, Design, and Applications*, New York: M. Dekker, 1989.
- [2] Schwarz, K. K., *Design of Industrial Electric Motor Drives*, Oxford, Boston: Butterworth-Heinemann, 1991.
- [3] Hugher, Austin, *Electric Motors and Drivers: Fundamentals, Types, and Applications*, Oxford, Boston: Newnes, 1993.
- [4] A. M. Trzynadlowski, *The Field Orientation Principle in Control of Induction Motors*, Kluwer Academic, 1994.
- [5] Novotny, D. W., *Vector Control and Dynamics of AC drives*, New York: Oxford University Press, 1997.
- [6] R. Jonsson, "Natural Field Orientation Provides Sensorless Control of AC Induction Servo Motors", *PCIM*, June 1995, pp. 44-51.
- [7] A. Hughes, J. Corda, D. A. Andrade, "Vector Control of Cage Induction Motors: a physical insight", *IEEE Proc, Electr. Power Appl.*, Vol. 143, No. 1, Jan 1996, pp. 59-68.
- [8] G. M. Liaw, F. J. Lin, "A Robust Speed Controller for Induction Motor Drives," *IEEE Trans, on Industrial Electronics*, Vol. 41, No. 3, June 1994, pp. 308-317.
- [9] P.C. Sen, "Electric Motor Drives and Control – Past, Present and Future", *IEEE Trans. on Industrial Electronics*, vol. 37, no. 6, Dec. 1990, pp. 562-575.

- [10] Shepherd, W., *Power Electronics and Motor Control*, Cambridge: Cambridge University Press, 1987.
- [11] Leksono, E., and Pratikto, "Adaptive Speed Control of Induction Motor with DSP Implementation", Industrial Electronics Society, IECON 2004. 30th Annual Conference of IEEE, Vol 2, 2-6 Nov. 2004, pp.1423 – 1428.
- [12] Rasmussen, H., Vadstrup, P., and Borsting, H. "Full Adaptive Backstepping Design of a Speed Sensorless Field Oriented Controller for an Induction Motor", IEEE/IAS Annual Meeting Conference Record, Oct. 2001, pp. 2601-2606
- [13] Tan, H., Technol., and Rockwell, "Field Orientation and Adaptive Backstepping for Induction Motor Control", Industry Applications Conference, Thirty-Fourth IAS Annual Meeting, Oct, 1999, vol 4, pp. 2357-2363.
- [14] Gyu-Sik Kim, Jae-Yoon Kim, Ju-Yeop Choi, and Ick Choy, "Recursive Rotor Resistance Adaptation Algorithm for Induction Motor Control", Industrial Electronics Society, IECON '98, Sep, 1998, vol 2, pp. 883-887.
- [15] Chiewchitboon, P., Tipsuwanporn, V., Soonthornphisaj, N., Piyarat, W., "Speed Control of Three-phase Induction Motor Online Tuning by Genetic Algorithm", Power Electronics and Drive Systems, PEDS, Nov, 2003, vol11, pp. 184-188.
- [16] M. N. Uddin, M. A. Abido, and M. A. Rahman, "Real-Time Performance Evaluation of a Genetic Algorithm Based Fuzzy Logic Controller for IPM Motor Drives", IEEE Transactions on Industry Applications, Jan./Feb. 2005, pp.
- [17] Siri Weerasooriya and M. A. El-Sarkawi, "Identification and Control of a DC Motor Using Back Propagation Neural Networks", IEEE Trans. On Energy conversion, vol. 6, no.4, Dec. 1991, pp. 663-669.

- [18] F.M. Khouly, A.S. A. Gaffar, A.A. Mohammed and A.M. Sharaf, "Artificial Intelligent Speed Control Strategies for Permanent Magnet DC Motor Drives", IEEE IAS Annual Meeting Conference Record, 1994, pp. 379-385.
- [19] M.A. Rahman and M.A. Hoque, "On-Line Self-Tuning ANN Based Speed Control of a PM DC Motor", IEEE/ASME Trans. On Mechatronics, vol. 2, No. 3, Sep, 1997, pp. 169-178.
- [20] M.T. Wishart and R.G. Harley, "Identification and Control of Induction Machines using Artificial Neural Network", IEEE/IAS Annual Meeting Conference Record, 1993, pp. 703-709.
- [21] B. Butron, R.G. Harley, G. Diana and J.L. Rodgerson, "Implementation of a Neural Network to Adaptively Identify and Control of VSI-Fed Induction Motor Stator Currents", IEEE Trans. on Industry Applications, vol. 34, no. 3, May/June 1998, pp. 580-588.
- [22] A. Ba-razzouk, G. Olivier and A. Cheriti, "A Neural Networks Based Field Oriented Control Scheme for Induction Motors", IEEE/IAS Annual Meeting Conference Record, 1997, pp. 807-811.
- [23] L. Ben-Brahim, K. Shimane, T. Kudor and H. Naitoh, "Implementation of an Inductance Motor Estimator using Neural Network", IPEC Conference Record, Japan, 1997, pp. 52-57.
- [24] B. Burton, F. Kamran, R.G. Harley, G.T. Habetter, M. Broike and R. Poddar, "Identification and Control of Induction Motor Stator Currents using Fast On-Line Random Training of a Neural Network", IEEE/IAS Annual Meeting Conference Record, 1995, pp. 1781-1787.

- [25] Ba-Razzouk, A., Cheriti, A., Olivier, G., and Sicard, P, "Field-oriented Control of Induction Motors using Neural-network Decouplers", IEEE trans, Power Electronics, Jul, 1997, Vol 12, pp. 752-763.
- [26] Tien-Chi Chen, and Tsong-Terng Sheu, "Model Reference Neural Network Controller for Induction Motor Speed Control", IEEE trans, Energy Conversion, Jun, 2002, Vol. 17, pp. 157-163.
- [27] L. A. Zadeh, "Outline of a new Approach to the Analysis of Complex System and Decision Processes", IEEE Trans. on Syst, Man and Cybern., vol. SMC3, 1973, pp. 28-44.
- [28] G. S. Buja, "Neural Network Implementation of a Fuzzy Logic Controller", IEEE/IECON Conference Record, 1993, pp. 414-417.
- [29] P. Lin, S. Hwang and J.Chou, "Comparison on Fuzzy Logic and PID Controls for a dc Motor Position Control", IEEE/IAS Annual Meeting Conference Record, 1994, pp. 1930-1935.
- [31] B. Singh, V. K. Sharma, and S. S. Murthy, "Performance Analysis of Adaptive Fuzzy Logic Controller for Switched Reluctance Motor Drive System", IEEE/IAS Annual Meeting Conference Record, 1998, pp. 571-579.
- [32] Golea, N., Golea, A., Boumehrez, M., and Kadjoudj, M., "Fuzzy Adaptive Approach to Nonlinear Systems Control", Industrial Electronics Society, IECON '01, Nov, 2001, Vol 1, pp. 782-786.
- [33] Uddin, M.N., Radwan, T.S., and Rahman, M.A., "Performances of Fuzzy-logic-based Indirect Vector Control for Induction Motor Drive", IEEE Trans, on Industry Applications, Sep/Oct, 2002, Vol 38, pp. 1219-1225.

- [34] E. Cerruto, A. Consoli, A. Raciti and A. Testa, "Fuzzy Addaptive Vector Control of Induction Motor Drive", IEEE Trans, on Power Electronics, vol. 12, No. 6, Nov. 1997, pp. 1028-1039.
- [35] S. A. Mir and D. S. Zinger, "Fuzzy Controller for Inverter Fed Induction Machines", IEEE/IAS Annual Meeting Conference Record, 1992, pp. 464-471.
- [36] Tae-Chon Ahn, Yang-Won Kwon, Hyung-Soo Hwang, and Pedrycz, W., "Design of Neuro-fuzzy Controller on DSP for Real-Time Control of Induction Motors", IFSA World Congress and 20th NAFIPS International Conference, Jul, 2001, vol. 5, pp. 3038-3043.
- [37] Kyu-Bock Cho, "A Neuro Fuzzy Controller for Inverter Fed Variable Speed Induction Motor Drive on the Power System", Neural Networks to Power Systems, ANNPS '93, Apr, 1993, pp. 47-52.
- [38] Alexandru, M., and Popescu, D, "Neuro-fuzzy Diagnosis in Final Control Elements of AC Motors", American Control Conference, Jul, 2004, Vol. 4, pp. 3759-3763.
- [39] Hao Wen, and Uddin, M.N. "Development of a Neuro-fuzzy Controller for Induction Motor", CCECE Conference record, 2004, vol. 3, pp. 1225-1228.
- [40] Uddin, M.N., and Wen, H. "Development of a Self-tuned Neuro-fuzzy Controller for Induction Motor Drives", IEEE/IAS conference record, Oct, 2004, pp. 2630-2636.
- [41] B. K. Bose, N. R. Patel and K. Rajashekara, "A Neuro-Fuzzy Based On-Line Efficiency Optimization Control of a Stator Flux-Oriented Direct Vector-

- Controlled Induction Motor Drive”, IEEE Trans. on Industrial Electronics, vol. 44, no. 2, Apr 1997, pp. 270-273.
- [42] Grabowski, P.Z., Kazmierkowski, M.P., Bose, B.K., and Blaabjerg, F, “A Simple Direct-torque Neuro-fuzzy Control of PWM-inverter-fed Induction Motor Drive”, IEEE Trans, on Industrial Electronics, Aug, 2000, Vol. 47, pp. 863-870.
- [43] A. Rubaai, D. Ricketts, and M. D. Kankam, “Development and Implementation of an Adaptive Fuzzy-Neural-Network Controller for Brushless Drives”, IEEE Trans. on Ind. Elec., vol. 38, no. 2, March/April 2002, pp. 441-447.
- [44] Krein, Philip T., *Elements of Power Electronics*, Oxford University Press, 1998.
- [45] Datta, S. K., *Power Electronics and Controls*, Reston Pub. Co., 1985.
- [46] Williams, B. W. *Power Electronics: Devices, Drivers, Applications, and Passive Components*, New York, McGraw-Hill, 1992.
- [47] Ali Zilouchian, and Mo jamshidi, *Intelligent Control Systems using Soft Computing Methodologies*, CRC Press LLC, 2001.
- [48] Schalkoff, Robert J., *Artificial Intelligence: an Engineering Approach*, New York, McGraw-Hill, 1990.
- [49] Bart Kosko, *Fuzzy Engineering*, Prentice-Hall, Inc, 1997
- [50] Skapura, David M. *Building Neural network*, ACM press, Addison-Wesley, 1996.
- [51] Mehrotra Kishan, *Elements of Artificial Neural Networks*, Cambridge, Mass: MIT Press, 1997.



- [52] Andrzej Piegat, *Fuzzy Modeling and Control*, Physica-Verlag Heidelberg, New York, 2001.
- [53] Matlab, *Simulink User Guide*, The Mathworks Inc, 2004
- [54] Marko Hinkkanen and Jorma Luomi, "Parameter Sensitivity of Full-Order Flux Observers for Induction Motors", *IEEE Trans. on Ind. Applications*, vol.39, no.4, Jul/Aug, 2003, pp. 1127-1135.
- [55] H. Tajima and Y. Hori, "Speed Sensorless Field-Orientation Control of the Induction Machine". *IEEE Trans.*, on IA, Vol. 29, no. 1 Jan/Feb 1993, pp. 175-180.
- [56] J. Holtz, "Methods for Speed Sensorless Control of AC Drives", in *Ssensorless Control of AC Motor Drives*, IEEE Press Book, 1996.
- [57] J. Maes et al., "Speed-sensorless Direct Torque Control of Induction Motors Using an Adaptive Flux Observer," *IEEE. Trans. on Industry Applications*, vol. 36, no.3, May-June 2000, pp. 778-785.
- [58] Patrick L. Jansen, and Robert D.Loren "A Physically Insightful Approach to the Design and Accuracy Assessment of Flux Observers for Field Oriented Induction Machine Drives", *IEEE Trans. on Ind. Applications*, vol.30, No.1, Jan, 1994, pp. 101-110.
- [59] M.Nasir Uddin, and Hao Wen, "Model Reference Adaptive Flux Observer Based Neuro-Fuzzy Controller for Induction Motor Drive", Accepted for *IEEE/IAS Annual Meeting Conference*, Hong Kong 2005.